Title

Enhancing Carbon Dioxide Desorption from Mono-ethanolamine Solutions through in-situ Mineralization and Generation of Calcium Carbonate Particles

Author

Al Aqeeli, Anas

Publication Date

2020

Peer reviewed|Thesis/dissertation

UNIVERSITY OF CALIFORNIA

Los Angeles

Enhancing Carbon Dioxide Desorption from Mono-ethanolamine Solutions through in-situ Mineralization and Generation of Calcium Carbonate Particles

A thesis is submitted in partial satisfaction

of the requirements for the degree of Master of Science

in Chemical Engineering

by

Anas Saleh N. Al Aqeeli

2020

ABSTRACT OF THE THESIS

Enhancing Carbon Dioxide Desorption from Mono-ethanolamine Solutions through in-situ Mineralization and Generation of Calcium Carbonate Particles

by

Anas Saleh N. Al Aqeeli

Master of Science in Chemical Engineering

University of California, Los Angeles, 2020

Professor Dante A. Simonetti, Chair

Improving processes' efficiency and reducing their carbon footprint is becoming more vital as the population and demand for energy increases. Today, carbon capture with amine solvents stands as the most effective and industrially applicable chemical separation technology demonstrated at a commercial scale due to their high absorption capacity and regenerability. However, aside from advantages that aqueous amine solutions offer, they suffer from the exceedingly high regeneration energy which is required to strip off the majority of absorbed CO_2. The objective of this work is to improve the regeneration process of a 22 vol.% mono-ethanolamine (MEA) solution by attempting to mineralize carbon dioxide using different solid calcium precursors namely $Ca(OH)_2$, $CaCl_2$, and CaO at low regeneration temperatures around 80^oC. The results show that adding stoichiometric amounts of $Ca(OH)_2$, CaO and $CaCl_2$ to balance the absorbed CO_2 in MEA while

heating the rich MEA solutions brought their CO_2 loading to below 0.045 mol CO_2/mol MEA ratio, which was much lower than 0.226 mol/mol in the case of thermal regeneration alone. In addition, the generation of solid $CaCO_3$ particles in MEA solutions by the partial mineralization of absorbed CO_2 has shown to improve both absorption and desorption kinetics. Overall, the study results proved the importance of the thermal energy in driving the mineralization reaction and thereby regenerating MEA. Moreover, the mineralization of captured CO_2 could become a potential industrial improvement as it combines capturing CO_2 in a thermodynamically stable form and leveraging a more chemically favored route for amine regeneration.

The thesis of Anas Saleh N. Al Aqeeli is approved.

Vasilios Manousiouthakis

Philippe Sautet

Dante A. Simonetti, Committee Chair

University of California, Los Angeles

2020

To my dad and mom,

my beloved wife, and my sweet daughter …

Table of Contents

List of Figures

List of Tables

Acknowledgement

First and foremost, I would like to thank the almighty Allah for all his blessings and for giving me the strength and endurance to complete this work.

I would like to express my immense gratitude and appreciation to my advisor Prof. Dante Simonetti for his invaluable advice and guidance throughout this journey. I would also like to thank my committee members Prof. Vasilios Manousiouthakis and Prof. Philippe Sautet for assessing and endorsing my work.

I would like to sincerely thank my research colleagues in the Simonetti's lab for their collaborative work, technical discussions, and for our joyful moments.

My deep thanks and gratefulness to my parents, my wife, and my brothers and sisters for their emotional support and encouragement. Their words have always echoed in my mind.

Finally, I would like to recognize Saudi Aramco for sponsoring my degree here at UCLA

Notation

$N_{CO_2,Li}$	Loaded CO_2 in MEA solution [mole]
$N_{CO_2,G}$	Moles of CO_2 desorbed to the gas phase [mole]
$N_{CO_2,Lf}$	Remaining CO_2 moles in MEA solution [mole]
J_{CO_2}	Molar flux of CO_2 [mol/(min.m$_2$)]
V_{N_2}	Volumetric flow rate of stripping N_2 gas during desorption [L/min]
V	The volumetric flow rate of the inlet gas [ml/min]
x	CO_2 molar fraction in the outlet gas [-]
n	Measurement step
P	Atmospheric pressure [atm]
Δt	Measurement steps time difference [min]
R	Gas constant [ml.atm/(mol.K)]
k_L:	Convective mass transfer coefficient in the liquid phase [mol/(min.m^2.atm)]
k_G:	Convective mass transfer coefficient in the gas phase [mol/(min.m^2.atm)]
C_{CO_2}:	Concentration of CO_2 in the bulk liquid phase [mol/L]
${C_{CO_2}}^i$:	Concentration of CO_2 in the liquid at the gas/liquid interface [mol/L]
${C_{CO_2}}^*$:	Concentration of CO_2 in the liquid at equilibrium with the partial gas pressure [mol/L]
P_{CO_2}:	Partial pressure of CO_2 in the bulk gas phase [atm]
${P_{CO_2}}^i$:	Partial pressure of CO_2 at the liquid/gas interface [atm]
${P_{CO_2}}^*$:	Partial pressure of CO_2 in equilibrium with the bulk liquid concentration [atm]
K_G:	Overall mass transfer coefficient based on the pressure driving force [mol/(min.cm^3.atm)]
m:	Henry's constant evaluated at the system's temperature [atm.L/mol]
E	Enhancement factor [-]
N_{max}	Maximum CO_2 absorption/desorption rate from solid-free MEA solution [mol/min]
$N_{max-solids}$	Maximum CO_2 absorption/desorption rate from MEA solution with 2 wt.% solids [mol/min]

1 Introduction

Greenhouse gases such as carbon dioxide, methane, nitrous and to fluorinated gases are known to cause a detrimental environmental impact. They act as a gaseous blanket that traps the heat in the atmosphere causing the surface temperature to rise. Carbon dioxide gas represents a majority of 82% of the total greenhouse gases emissions in the United States in 2017 with nearly 33% of total emission coming from power generation plants that burns coal and natural gas (US EPA, n.d.). Recent studies concerning carbon dioxide emissions suggests that the global CO_2 emissions are drastically rising from 33.1 Gigatons in the year of 2010 to 37.1 Gigatons in 2018 – nearly 7.5% increase in less than a decade ("Global Carbon Project (GCP)," n.d.). In response to the dramatic CO_2 emission increase, global consents were gathered by United Nations Framework Convention on Climate to strengthen the response to the threat of climate change in what was known as "Paris agreement" back in 2015. The agreement entailed reaching common grounds among participating parties mainly focusing on lowering greenhouse gas emissions to hold the global average temperature to well below 2 ^oC above pre-industrial levels and setting 1.5 ^oC as a target (Zhong et al. 2010). To coop with the agreement terms and sustain a secure source of energy for the growing population, power generation plants and other major CO_2-emitting sources needs to become more energy efficient and to have less carbon footprint. Among the exhausted efforts to achieve this goal, Carbon Capture and Sequestration (CCS) stands as a widely considered approach capable of reducing CO_2 emissions (typically 85-90%) from large emission point sources such as power plants (Leung, Caramanna, and Maroto-Valer 2014).

Captured CO_2 through CCS can be classified into three main categories (figure 1): post-combustion CO_2, pre-combustion CO_2, and oxyfuel combustion generated CO_2 (Dutcher, Fan, and

Russell 2015; Koytsoumpa, Bergins, and Kakaras 2018). In pre-combustion, CO_2 is captured in the synthesis gas after converting CO to CO_2 and H_2 through the well-known water-gas-shift reaction. Post-combustion captures CO_2 in the exhaust gases after completely burning fuel in air. Oxy-combustion technologies mainly consider burning fuel in pure oxygen and recycling the exhaust gases. Depending on the source and concentration of CO_2 in the treated gas, suitable chemical (such as amine absorption) or physical (such as the use of membranes or cryogenic separation) separation methods can be used. High partial pressures of CO_2 in a given gas stream make the separation process much easier allowing the CO_2 to be readily separable by physical processes (Koytsoumpa, Bergins, and Kakaras 2018). However, low CO_2 partial pressures makes the gas separation more difficult and would require more stringent chemical separation methods (Koytsoumpa, Bergins, and Kakaras 2018). Figure 2 summarizes the main CO_2 capture technologies.

Nowadays, post-combustion carbon capture with amine solvents stands as the most effective and industrially applicable chemical separation technology demonstrated at a commercial scale (Rochelle 2009; Koytsoumpa, Bergins, and Kakaras 2018; Dutcher, Fan, and Russell 2015). This is particularly true considering the low CO_2 concentration present in the treated gas. For example, CO_2 concentration from air coal combustion plants ranges from 12 – 15% whereas it can go as low as 3% in flue gases from natural gas combustion (Koytsoumpa, Bergins, and Kakaras 2018). Various amines are known for their effective performance in capturing CO_2 from flue gas streams and their choice depends on their distinctive properties. For instance, chemical absorption using primary amine aqueous solutions are preferred over other types of amines due to their high reaction kinetics towards capturing CO_2 (Kanniche et al. 2010). On the other hand, tertiary amines have slower reaction kinetics and capacities but they are much easier to regenerate than primary

amines (Rinprasertmeechai et al. 2012). Generally, the choice of the appropriate amine is an optimization exercise that requires weighing the desired properties against the separation process conditions.

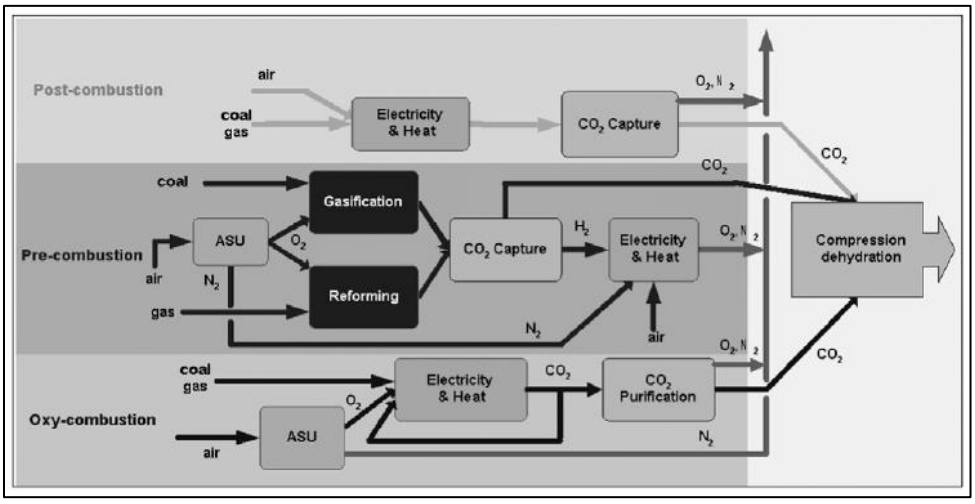

Figure 1: The three main CO_2 capture processes (Kanniche et al. 2010)

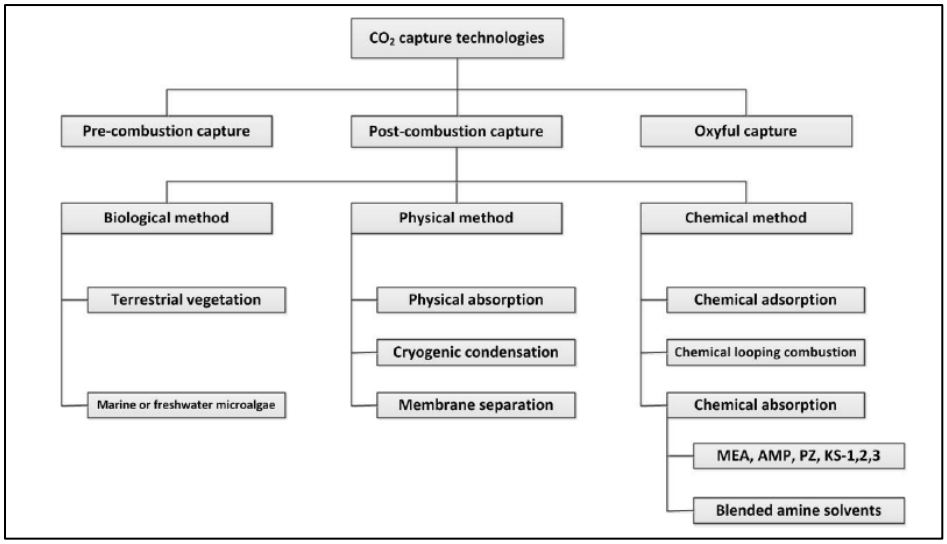

Figure 2: Technology options for CO_2 capture (Wu et al. 2014)

2 Background

2.1 Chemical CO_2 absorption by amines

The reaction of CO_2 gas with aqueous amine solutions is known to proceed through a zwitterion mechanism which was originally proposed by Caplow in 1968 (Caplow 1968). It involves the reaction of amines, whether primary (RNH_2) or secondary (R_1R_2NH), with carbon dioxide to form a zwitterion which can spontaneously react with any base (B) to form carbamate ion and a protonated base.

$$CO_2 + RNH_2 \rightarrow RNH_2{}^+COO^- \quad (1)$$

$$RNH_2{}^+COO^- + B \rightarrow RNHCOO^- + B^+ \quad (2)$$

$$CO_2 + R_1R_2NH \rightarrow R_1R_2NH^+COO^- \quad (3)$$

$$RNH^+COO^- + B \rightarrow RNCOO^- + B^+ \quad (4)$$

The base that deprotonates the carbamate ions in equations (2) and (4) could be H_2O, OH^- or another amine (Putta et al. 2016). The latter case is applicable to primary and secondary amines giving the overall reaction (for primary amine in this case) as in equation (5) and limiting the molar absorption capacity to 0.5 mole CO_2 per mole of amine (Huertas et al. 2015).

$$2\,RNH_2 + CO_2 \rightarrow RNHCOO^- + RNH_3{}^+ \quad (5)$$

At high concentrations of CO_2 in amine solutions, unstable carbamate tends to hydrolyze to bicarbonate and amine thereby bringing the nominal absorption capacity to 1.0 mole CO_2 per

mol amine as described in equation (6). However, tertiary amine can't form carbamate but rather undergoes a direct CO_2 hydration as in equation (7) (Lv et al. 2015).

$$RNH_2 + CO_2 + H_2O \leftrightarrow RNH_3^+ + HCO_3^- \quad (6)$$

$$R_1R_2R_3N + CO_2 + H_2O \leftrightarrow R_1R_2R_3NH^+ + HCO_3^- \quad (7)$$

Jakobsen et al. studied the liquid phase composition of 30 vol% mono-ethanolamine (MEA) solution when loaded with different amounts of CO_2 using Nuclear Magnetic Resonance (NMR) (Jakobsen, Krane, and Svendsen 2005). In their experiments, they used special pressure/vacuum sample tubes filled with 0.4 ml of 30 wt.% MEA solution (made by mixing 99% purity MEA liquid with deionized water). The sample tubes were connected to an apparatus that evacuates and cools the tubes in a liquid nitrogen bath. After evacuation, pure $^{13}CO_2$ gas sent from a sealed reservoir with a known pressure was allowed to fill the sample tube until the reservoir pressure equilibrates. The sample tubes were then sealed and heated to 20^{o}C for 1 hour before collecting the NMR spectra at the same temperature. The volume of the reservoir and the pressure changes where used to calculate the amount of gas in the sample tubes and the spectral peak areas where used to measure to the respective species concentrations. Figure 3 shows the concentration profile of various aqueous species versus the molar CO_2 loading per moles of MEA in solution. The results in figure 3 clearly show that protonated amines are the major products produced during the initial stage of absorption with bicarbonates evolving on the expense of carbamates at loadings higher than 0.5 mol CO_2/mol MEA.

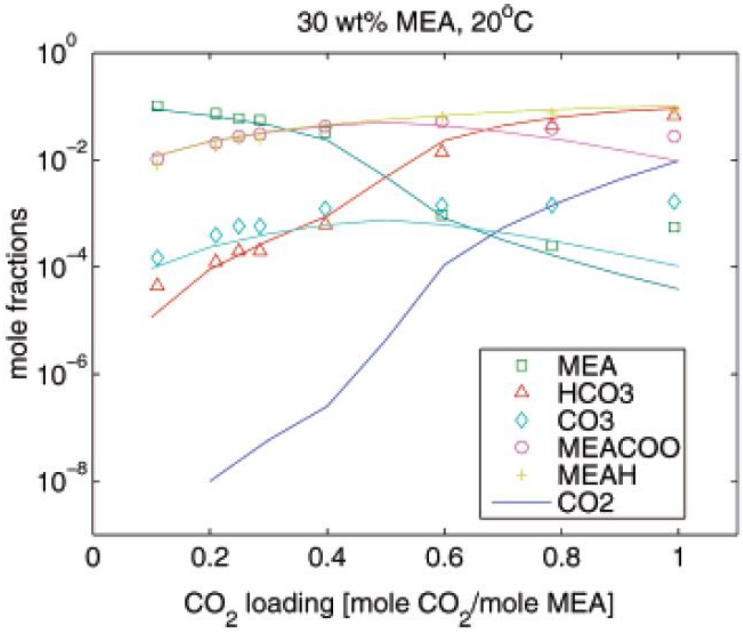

Figure 3: Liquid phase speciation for 30% MEA solution at 20 °C (Jakobsen, Krane, and Svendsen 2005)

Some of the important equilibrium reactions taking place during CO_2 absorption in amines aqueous solutions are (Jakobsen, Krane, and Svendsen 2005):

Dissociation of water:

$$H_2O \leftrightarrow H^+ + OH^- \tag{8}$$

Dissociation of carbon dioxide:

$$CO_2 + H_2O \leftrightarrow HCO_3^- + H^+ \tag{9}$$

Dissociation of bicarbonate ion by a base (water in this case):

$$HCO_3^- + H_2O \leftrightarrow CO_3^{2-} + H_3O^+ \tag{10}$$

Dissociation of protonated amine by a base:

$$amineH^+ + H_2O \leftrightarrow amine + H_3O^+ \quad (11)$$

Carbamate reversion to bicarbonate:

$$amineCOO^- + H_2O \leftrightarrow amine + HCO_3^- \quad (12)$$

By observing the sequence of reactions in figure 3, which considers the primary amine MEA, it can be drawn that at the loading capacity of 0.5 mol CO_2/mol MEA there exist equimolar amounts of carbamate and protonated amines species. However, when the CO_2 loading increases further, and the solution's pH becomes more acidic, the reverse direction of reactions (10) and (11) and the forward direction of reaction (12) starts to dominate resulting in the conversion of carbamate and bicarbonates to protonated amine and carbonates. In addition to the rising pH when saturating amine solution with CO_2, the temperature of the solution also increases due to the exothermic absorption reaction (Lv et al. 2015). As depicted in figure 4, the rise in temperature is proportional to CO_2 molar loading until a point where exothermicity start to decline above 0.5 mol CO_2/mol MEA loading.

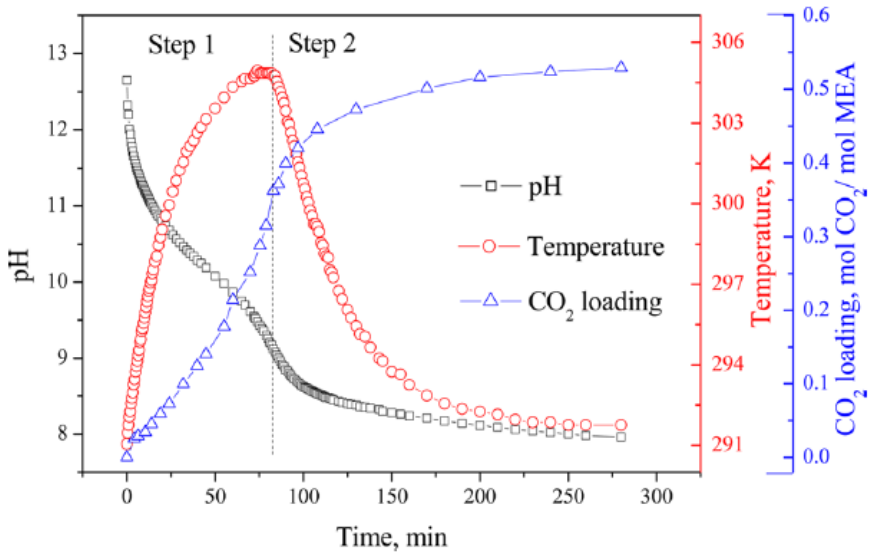

Figure 4: Performance of CO_2 absorption in 30 vol% MEA solution (Lv et al. 2015)

2.2 Chemical CO_2 desorption by amines

Amine regeneration is a process of reversing CO_2 absorption reaction by heating the rich amine solutions to a boiling temperature. Amine regeneration reactions, particularly for primary amines such as MEA, can be categorized into A) carbamate breakdown (equation (13)) and B) protonated amine deprotonation (equation (14)) with estimated heat of regeneration of 15.5 kJ.mol^{-1} and 78.2 kJ.mol^{-1} at 90 ^{o}C, respectively (Shi et al. 2014).

$$AmineCOO^- + H_3O^+ \leftrightarrow Amine + CO_2 \uparrow + H_2O \qquad \Delta G \sim 15.5\ kJ.mol^{-1} \qquad (13)$$

$$AmineH^+ + H_2O \leftrightarrow Amine + H_3O^+ \qquad \Delta G \sim 78.2\ kJ.mol^{-1} \qquad (14)$$

From the difference in energy requirement between the above two reactions, it is clear that most of the energy required is for the deprotonation of amine rather than breaking down carbamate.

However, carbamate breakdown has been found to be largely dependent on the availability of free protons and because a CO_2-saturated amine typically has a pH in the range of 8 - 10, there is a clear shortage of free protons available for this reaction to proceed (Shi et al. 2014). In the absence of external source of free protons (by adding acid for example), reaction (14) becomes the main reaction that gives away free protons necessary for breaking down carbamate. Moreover, as saturated amine becomes rich in carbonate and (to a less extent) bicarbonate, the decreased alkalinity of the solution drives reactions (9) and (10) in the reverse direction resulting in more desorbed CO_2 gas.

3 Literature Review

3.1 CO_2 capture in amine solutions

Coal-fired power plants in the United States have an electric power capacity that is high enough to supply nearly 50% of the total power generated in the country and this in turn contributes to more than 30% of the CO_2 emissions (Rochelle 2009). Due to the increase in energy demand resulting from the fast-growing population and the lack of industrial maturity of non-fossil fuel power-generation technologies, the dependence on fossil fuel sources for power generation is expected to remain and reasonable climate change actions should center around reducing their emissions without shutting them down (Rochelle 2009). Nowadays, amine scrubbing is considered the main technology for post-combustion CO_2 capture due to its high absorption capacity and stability (Dutcher, Fan, and Russell 2015). Some of the commonly used amines for CO_2 scrubbing process include the primary amine mono-ethanolamine (MEA), the secondary amine

diethanolamine (DEA) and the tertiary amine triethanolamine (TEA), the sterically hindered amine 2-amino-2-methyl-1-propanol (AMP) and peprazine (PZ). Amines are highly regarded as ideal chemical absorbents for CO_2 capture due to their high cyclability, capacity and regenerability (Koytsoumpa, Bergins, and Kakaras 2018; Hamidi, Farsi, and Eslamloueyan 2018; Tong et al. 2012).

In a typical CO_2 amine scrubbing process in a power-generation plan, the flue gas is sent to a scrubbing column where the lean aqueous amine solution absorbs CO_2 and becomes a rich amine stream. The CO_2-rich amine is then pumped to a stripping column where it gets heated to strip out CO_2 and become a lean amine steam. Afterwards, the captured CO_2 gas is compressed in preparation for storage and further sequestration (Dutcher, Fan, and Russell 2015). The process continues by recycling the lean amine back to the absorber to absorb CO_2 from the flue gas again. Figure 5 shows a scheme for a typical amine scrubbing process.

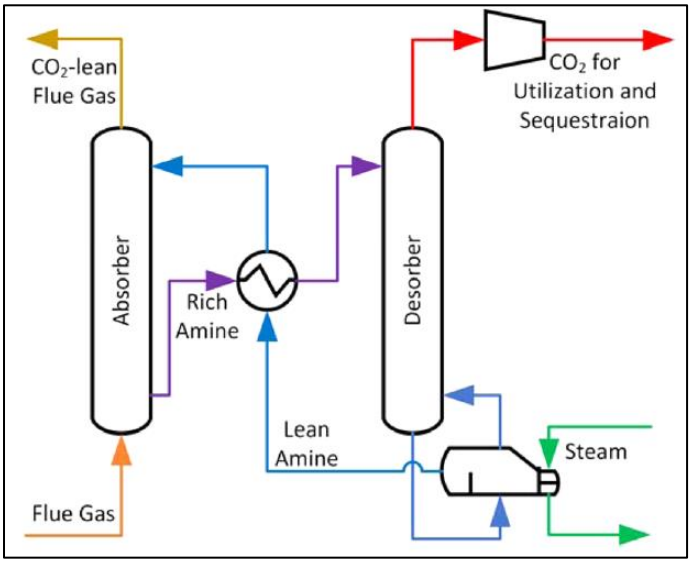

Figure 5: Typical CO_2 amine scrubbing process (Dutcher, Fan, and Russell 2015)

3.1.1 CO_2 capture in mono-ethanolamine (MEA)

Mono-ethanolamine (MEA) is a colorless liquid that has numerous commercial applications where it could be used as softening agent for hides, an agricultural chemical dispersant, a cosmetic polisher, and to synthesize specialized surface-active agents (McCant 2015). Table 1 summarizes the physical properties of MEA. On the industrial level, MEA aqueous solutions are primarily used for the removal of carbon dioxide and hydrogen sulfide from natural gas and other flue gases. Some of the advantages pertaining to MEA solutions is their fast kinetics towards the reaction with CO_2, high regenerability, and relatively low cost of raw materials (Mondal 2009; Lv et al. 2015). CO_2 absorption in amines is an exothermic reaction that gives off thermal energy resulting in a temperature increase. The thermal energy given off by MEA absorption is generally higher than those from other secondary or tertiary amines, which is indicative of a more energetic reaction that results in a more stable absorption products in solution (Kim et al. 2013). As such, MEA is most efficient in maintaining a high absorption capacity at elevated temperatures compared to other amines which tends to lose significant capacity (Kim et al. 2013). Besides MEA being a superior absorbent, it has some inherent disadvantages such as high regeneration energy and relatively low absorption capacity. Therefore, in pursuit of utilizing the superior benefits of MEA solutions, current research efforts are centered around making MEA absorption and desorption processes more energy efficient and less costly.

Table 1: Physical properties of MEA (McCant 2015)

Parameter	Value
Molecular formula	C_2H_7NO
Structural formula	$HOC\text{-}CH_2\text{-}CH_2\text{-}NH_2$
Physical State	Liquid
Color	Colorless
Solubility in water	1×10^6 mg/L
Molecular weight	61.08 g/mol
Boiling point	170.8 ^oC

3.1.2 CO_2 capture in other amines and their mixtures

The variety of amine structures and chemical properties brings about an array of choices when it comes to selecting a suitable amine for a specific application. For example, tertiary amines such as TEA exhibits very slow absorption kinetics and has very limited temperature tolerance compared to MEA. However, the regeneration energy for TEA solution is about 50% of that for MEA (Kim et al. 2013). Moreover, TEA is known to have a much higher cyclic regeneration efficiency compared to MEA (Rinprasertmeechai et al. 2012). Sterically hindered amines are another attractive CO_2 absorbents due to their high absorption capacity (approaching 1.0 mol CO_2/mol amine) and lower regeneration energy compared to MEA (Tong et al. 2012; Kim et al. 2013). However, sterically hindered amines such as AMP suffers from slow reaction kinetics as opposed to MEA. Piperazine (PZ) is another studied amine with superior absorption capacities reaching above 1.0 mol/mol ratio and has much higher absorption rates than MEA (Adeosun et al. 2013). Although PZ provides superior capture benefits when blended with other amines, the tendency for PZ to crystallize at high blending concentrations is one of the reasons that limits their use (Adeosun et al. 2013). In an effort to synergies various amine properties, mixtures of different amines have been extensively investigated in literature (Rinprasertmeechai et al. 2012; Mondal 2009; Adeosun et al. 2013; Pacheco, Kaganoi, and Rochelle 2000; Hamidi, Farsi, and Eslamloueyan 2018; Zhang et al. 2018). For example, the absorption capacity of MEA can be

increased by mixing with PZ while still maintaining high absorption rates (Rinprasertmeechai et al. 2012).

3.2 Methods to enhance CO_2 desorption from amines

3.2.1 pH swing

It is thermodynamically true that increasing the pH of the saturated amine solution will shift the equilibrium of reaction (5) in the reverse direction favoring the CO_2 desorption. pH swing is a concept that is anticipated to help reduce the regeneration energy of CO_2-loaded amines by inducing an equilibrium change (Feng et al. 2010; Du 2017; Du et al. 2012). Feng et al reported the use of three weak organic acids (suberic acid, phthalic acid and oxalic acid) to facilitate the desorption of CO_2 from mono-ethanolamine (MEA), diethanolamine (DEA) and methyldiethanolamine (MDEA) (Feng et al. 2010). While adding acids to the absorbed amines, they observed an instantaneous CO_2 generation along with a significant heat release. Du et al. did similar investigation using four weak organic acids (adipic, phthalic, suberic and sebacic acids) to desorb CO_2 from the same three solvents. They observed that different acids would release different amounts of CO_2 proportional to the amount of acid added. However, none of the above studies reported a commercially feasible way of recovering the added acid or further investigated the effect of the acid addition on amines. Moreover, these studies suggested that the significant CO_2 release was more due to the spontaneous temperature rise of the solution caused by the acid reaction than by pH change.

There is very limited information in literature regarding the use of strong acids, such as hydrochloric acid, to induce a pH change and facilitate CO_2 desorption of amine (Lv et al. 2015).

Besides, strong acids finds extensive applications especially in titration to either confirm amine solution concentration (Akachuku et al. 2019; Osei et al. 2017) or the amount of CO_2 in loaded amines (Zhang et al. 2018; T. Wang et al. 2016). Other studies report hydrochloric acid to cause amine degradation when present in amine mixtures (Mondal 2009; Huertas et al. 2015). However, there doesn't seem to be enough evidence on how this deactivation happens or how it might change the chemical integrity of amines.

3.2.2 Adding solids

The use of solid nanoparticles such as SiO_2, TiO_2 and AlO_3 has been observed to remarkably improve the gas-liquid mass transfer coefficient for the amine absorption and desorption processes by reducing the liquid-side-mass-transfer-resistance (T. Wang et al. 2016; Jiang et al. 2014). Under similar desorption conditions, Wang et al showed that adding 0.1 wt% TiO_2 nanoparticles to MEA solution resulted in 42% faster desorption compared to solid free solutions. They explained this improved desorption by the combined mass transfer and heat transfer enhancements caused by nanoparticles addition, which were evident by the increase in the CO_2 desorption rates of the MEA solutions with the solid particles over those without the solids while using the same heat flux. They also observed that increasing the heating flux while maintaining the solvent temperature at 103 ^oC significantly reduced the CO_2 desorption time and magnified the mass transfer improvement caused by nanoparticles. Moreover, their results also showed that the bubble breaking effect of nanoparticles resulted in a notable increase in the effective gas-liquid interfacial surface area especially during CO_2 absorption in MEA. However, the nanoparticle addition was limited to less than 2 g/L to avoid the effect of increased fluid viscosity which could greatly hinder the effective mass transfer. Recently, there has been reports

on the use of solid acid catalysts to improve the absorption and desorption cycles of amines (Shi et al. 2014; Zhang et al. 2017, 2018; Akachuku et al. 2019). By using ZSM-5 catalyst as a Bronsted acid catalyst and gamma-Al_2O_3 as a Lewis acid catalyst, Shi et al (Shi et al. 2014) were able to obtain greater CO_2 production rates of 0.118 and 0.106 mol CO_2/mol MEA/h, respectively as compared to 0.074 mol CO_2/mol MEA for the solid-free solution of (5M) MEA. They explained the enhancement by the proton donor property in ZSM-5 which aid in breaking down carbamate and by the electron acceptor property in gamma-Al_2O_3 which facilitates bicarbonates generation. Zhang et al (Zhang et al. 2017) used SAPO-34 and SO42-/TiO2 solid catalysts enhance the CO_2 desorption from MEA. Using solid catalysts of up to 35 g/L loading, they quantified around 14 - 24% less energy consumption per mol CO_2 released compared to solid-free saturated MEA. Such mass transfer enhancement was considered crucial especially when absorbing CO_2 with a 12 vol% in the treated gas - a composition that mimics a typical power plant's flue gas.

Few mass-transfer theories have been proposed to explain the mechanism of nanoparticle enhancement in the absorption/desorption cycle of amines. Such theories include bubble breaking, shuttle effect, and boundary mixing effect (T. Wang et al. 2016; Jiang et al. 2014). The shuttle effect assumes that some suspended particles could absorb certain amount of gas and carries it across the gas-liquid boundary resulting in a facilitated gas transfer process. The boundary mixing effect assumes that particles inside the boundary layer could affect the hydrodynamics of the transfer process leading to enhanced mass transfer. The bubble breaking mechanism considers the breaking of gas bubbles by nanoparticle collision resulting in a larger gas-liquid contact area. However, there seems to be a distinct contribution of the three effects depending on the experimental conditions. For example, Wang et al (T. Wang et al. 2016) observed that adding nanoparticles into a bubble column of MEA solution undergoes different enhancement stages

depending on the CO_2-loading. The lean MEA loaded with nanoparticles showed better absorption rates compared to unloaded solution. In the stage where the MEA solution becomes richer in CO_2, they observed a reduction in enhancement possibly caused by nanoparticles hindering CO_2 mass transfer due to increased solution viscosity and particles agglomeration. In addition, their measurement of the zeta potential of MEA solutions with different loadings showed that at loadings above 0.3 mol CO_2/mol MEA the repulsion forces among the nanoparticles was significantly reduced indicating their instability and tendency to agglomerate. Moreover, their analysis suggested that at low particles loading (and lower viscosity) the shuttle effect and the boundary mixing effects made greater contribution to the enhancement of the mass transfer coefficient, whereas increasing the solid content made bubble breaking effect dominates the mass transfer process.

3.2.3 Mineralization/precipitation of CO_2

3.2.3.1 CO_2 mineralization

Carbon capture and sequestration (CCS) technologies aims at reducing the greenhouse gas emissions by capturing CO_2 from a large point source such as coal-fired gas plants. Geological CO_2 storage, or in situ mineral carbonation, has been widely recognized as a feasible process of capturing CO_2 (Chang et al. 2017). In this scheme, CO_2 can be injected into saline aquifer which could react with alkaline minerals present in the geological formation forming mineral carbonates such as $CaCO_3$ and $MgCO_3$. On the other hand, ex situ mineral carbonation is a process where CO_2 undergoes a serious of chemical reactions with alkaline earth metals such as magnesium and calcium which are extracted from different natural or industrial sources. Because mineral

carbonates such as $CaCO_3$ and $MgCO_3$ are the most thermodynamically stable form of carbon, long term CO_2 storage can be achieved in this process (Chang et al. 2017).

As one of the most common forms of carbonates, $CaCO_3$ is a polymorphic material that has three anhydrous crystalline phases (ranked in the order of decreasing stability) namely; calcite, aragonite and vaterite (Declet, Reyes, and Suárez 2016). Process parameters such as temperature, pH and ionic strength play important roles in determining the structure and phase of calcium polymorph during precipitation. In general, lower temperatures (15 – 30 ^oC) favor the formation of vaterite whereas higher temperatures (60 – 80 ^oC) favors forming the more stable calcite and aragonite polymorphs. Also, calcite is favorably formed at pH > 11 while aragonite becomes dominant at the pH range of 9 – 11. Vaterite mostly prevail at pH values lower than 8. Moreover, and apart from the temperature and pH effects, higher ionic strength was found to increase aragonite yield on the expense of calcite (Chang et al. 2017).

Some studies reported precipitating gaseous CO_2 in aqueous phases using calcium containing precursors such as calcium hydroxide (Velts et al. 2011). Some of the proposed reactions that CO_2 undergoes while converting to $CaCO_3$ in an aqueous mixture of $Ca(OH)_2$ includes:

$$Ca(OH)_2 \leftrightarrow Ca^{2+} + 2\,OH^- \quad (15)$$

$$CO_2 + OH^- \leftrightarrow HCO_3^- \quad (16)$$

$$HCO_3^- + OH^- \leftrightarrow CO_3^{2-} + H_2O \quad (17)$$

$$Ca^{2+} + CO_3^{2-} \leftrightarrow CaCO_3 \quad (18)$$

Velts et al. (Velts et al. 2011) modeled the precipitation process of $CaCO_3$ in a continuously stirred tank and by bubbling CO_2 in an aqueous solution containing $Ca(OH)_2$ as shown in figure 6. Their model estimated the kinetics of carbonate formation and CO_2 mineralization in reactions (17) and (18) to be 6.0×10^9 and 1.88×10^6 L/mol/min, respectively. These values were orders of magnitude higher than the kinetics of the conversion of gaseous CO_2 into bicarbonate in reaction (15) which had the value of 8.4×10^3. These values suggest that CO_2 mineralization by Ca^{2+} ions is a spontaneous reaction provided that HCO_3^- is readily available for reaction (17). However, and as can be seen in figure 6, $CaCO_3$ formation is also heavily dependent on the solution's pH. As the solution becomes more acidic, $CaCO_3$ becomes less stable and tends to decompose in the reverse direction of reaction (18) (Declet, Reyes, and Suárez 2016).

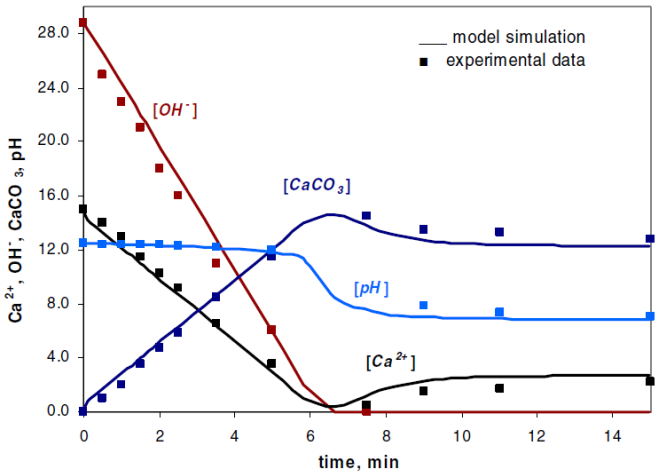

Figure 6: Modeled liquid concentration profiles for CO_2 bubbling in aqueous solution of $Ca(OH)_2$ (Velts et al. 2011)

3.2.3.2 Integrated CO_2 capture and precipitation in amines

Driven by the opportunity to make the CO_2 capture more energy efficient (by reducing the regeneration energy) and the desire to capture it in a stable and environmentally friendly form,

recent studies attempted precipitating CO_2 while captured in amine solutions (W. Wang et al. 2013; B. Yu et al. 2018; Ji et al. 2018). Amines are inherently superior chemicals that effectively absorbs CO_2 in high capacity. Precipitating CO_2 in amines takes advantage of the availability of large amounts of dissolved CO_2 and the spontaneous mineralization reaction. Generally, the CO_2 loading of amines can be brought to significantly lower values than their maximum loading capacity by mixing the rich amines with calcium containing precursors, such as $CaCl_2$ (Arti et al. 2017) and CaO (Ji et al. 2018) while capturing the dissolved CO_2 into stable $CaCO_3$ at temperatures as low as 40 ^oC.

Long Ji et al (Ji et al. 2018) reported mineralizing dissolved CO_2 in MEA, DEA and PZ amines using fly ash and reagent grade CaO solids. All their considered amines were bubbled with a 9% CO_2 in N_2 gas mixture until reaching their maximum CO_2 loading capacities. The saturated amines were then mixed in a 1.0 mol/mol ratio with CaO or fly ash at 40 ^oC. Their results show that CO_2 loadings of all the saturated amines (at 2 mol/L concentration) could be significantly reduced. For example, the CO_2 loading capacities of DEA and PZ amine solutions were brought from 0.53 and 0.79 to 0.1 and 0.07 mol/mol, respectively. However, following their mineralization process, MEA was regenerated to a much lesser extent reducing the capacity from 0.51 to only 0.31 mol/mol (Figure 7). Their analysis proposed that this lower regeneration efficiency was associated with the high stability of carbamate in MEA at lower CO_2 loadings which was supported by the persistent carbamate peaks appearing in the FT-IR spectrum after mineralization (Figure 8).

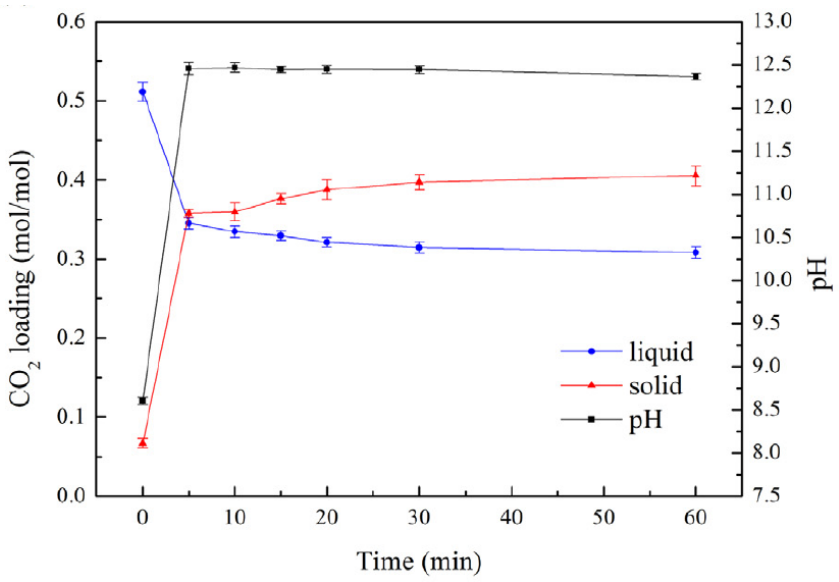

Figure 7: Regeneration of saturated MEA with 1.0 mol/mol of fly ash (Ji et al. 2018)

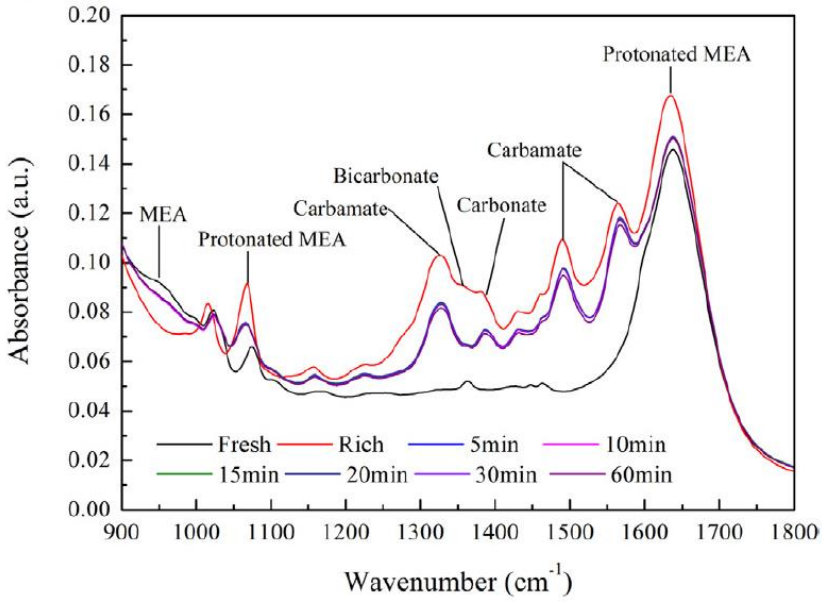

Figure 8: FT-IR spectrum of MEA solution regenerated with 1.0 mol/mol fly ash (Ji et al. 2018)

Another recent study by Arti et al. (Arti et al. 2017) reported the mineralization of CO_2 in different amine solutions using calcium chloride. They compared the thermal regeneration at 90 ^oC with the mineralization using anhydrous $CaCl_2$ at 40 ^oC for four different 1.6 mol/L amine

solutions of MEA, DEA MDEA and AMP. The mineralization method was found to significantly reduce the CO_2 loading in all amines compared to the thermal regeneration. For example, the thermal regeneration of MEA at 90 ^oC reduced the CO_2 loading from 0.66 to 0.44 mol CO_2/mol MEA. Whereas their results claimed that mixing the rich MEA solution with stoichiometric amount of $CaCl_2$ brought the lean loading to less than 0.02 mol CO_2/mol MEA. However, the mass yield of $CaCO_3$ indicated that less than 27% of calcium was converted to calcium carbonate.

4 Experimental Section

This section covers the experimental part to test the absorption enhancement through CO_2 capture in amine solutions. Specific sections include quantifying the absorption capacity of MEA and comparing it with literature values, attempting to mineralize CO_2 in MEA solutions using different calcium precursors, modeling the absorption and desorption/mineralization processes using a simplified Aspen Plus® model, and finally quantifying the absorption/desorption enhancements by the presence of $CaCO_3$ solid particles from the partial mineralization of CO_2.

4.1 Materials

22 vol% mono-ethanolamine (MEA) in water solution was purchased from Aqua Solutions Inc. and was used as the primary amine solvent in all experiments. Anhydrous calcium hydroxide ($Ca(OH)_2$) and Calcium chloride hydrate ($CaCl_2$) both purchased from Sigma-Aldrich were used as calcium precursors for the CO_2 mineralization. Calcium oxide was purchased from Merck in the form of small lumps and was crushed to obtain CaO particles with less than 80 mesh size (177

microns). Calcium carbonate fine solids in calcite form was purchased from Sigma-aldirch and was used as inert solid in the experiments that measure enhancements by the addition of solid particles.

4.2 Characterization

4.2.1 Gas phase Fourier transformation infrared spectroscopy (FT-IR)

The composition of the effluent gas from the reactor during each absorption/desorption step was measured using gas phase MKS Multigas^{TM} FT-IR analyzer. As necessary, the inlet flow to the FT-IR was diluted with a predetermined flow of ultra-high purity N_2 to bring the concentrations of analyzed gases to a lower and more accurate detection limit. The final CO_2 concentration was obtained by normalizing with the feed concentration value.

4.2.2 Liquid phase Fourier transformation infrared spectroscopy (FT-IR)

The liquid samples of MEA solutions were analyzed using Perkin Elmer FT-IR spectrometer with a scanning resolution of 0.5 cm^{-1}. Using a sample of 0.1 ml, this technique was used to qualitatively determine the composition of MEA solutions after undergoing different regeneration conditions. The component peak identification was done following the method used by Long ji et al (Ji et al. 2018).

4.2.3 pH analysis

Measurement of the pH for the liquid MEA solutions after different stages of regeneration and chemical treatment was done using Orion Star A211 pH meter obtained from Thermo Scientific. The equipment was calibrated with three Thermo Scientific Orion Application solutions with pH values of 4.01, 7.00 and 10.01.

4.2.4 Thermogravimetric Analyzer (TGA)

The precipitated solid samples in MEA solutions were analyzed using STA 6000 Perkin Elmer Thermogravimetric Analysis (TGA). The solids were collected by centrifuging the liquid mixtures at 4000 rpm for 10 minutes. Then, the collected solids were washed 3 times with deionized water before drying overnight at 110 ^{o}C. The dried solid samples were crushed into fine powder and around 27 g of the samples were transferred into a pure aluminum oxide crucible placed in a micro scale. Each sample was heated from 35 to 950 ^{o}C in a 15 ^{o}C/min temperature ramp under a flow of 20 ml/min of Ultra-Pure N_2 gas. The CO_2 loading of the solid samples was measured as the weight loss over the temperature range from 600 – 900 ^{o}C (Galan, Glasser, and Andrade 2013).

4.2.5 X-ray diffractometer (XRD)

Powder XRD patterns were obtained on X-ray diffractometer JEOL JDX-3530 and Philips X-Pert using Cu Kα radiation of 1.54 Å and a rotation angle of 20-60^{o}. The diffraction patterns were analyzed using Profex software to identify and confirm $CaCO_3$ phases in the solid samples.

4.3 Experiment setup and conditions

A rig was constructed to enable a real-time measurement of the CO_2 absorption and desorption rates in MEA solutions with the ability to heat the solution to a specific temperature. The schematic description of the experimental rig is shown in figure 9 and it consists of the following:

1. 250 ml three-neck round bottom beaker with a stirring bar

2. Allinh type glass condenser running deionized water and maintaining the temperature at 6 ^{o}C and installed in the gas outlet
3. A liquid chiller that circulates water at 6 ^{o}C through the glass condenser
4. A reactor gas inlet that receives N_2 and CO_2 inlet gases coming from two different gas cylinders and controlled by two MKS Multigas^{TM} mass flow controllers
5. Water bath placed over a hot plate equipped with temperature control and a magnetic stirrer
6. MKS Multigas^{TM} FT-IR analyzer to measure the CO_2 content in the outlet gas

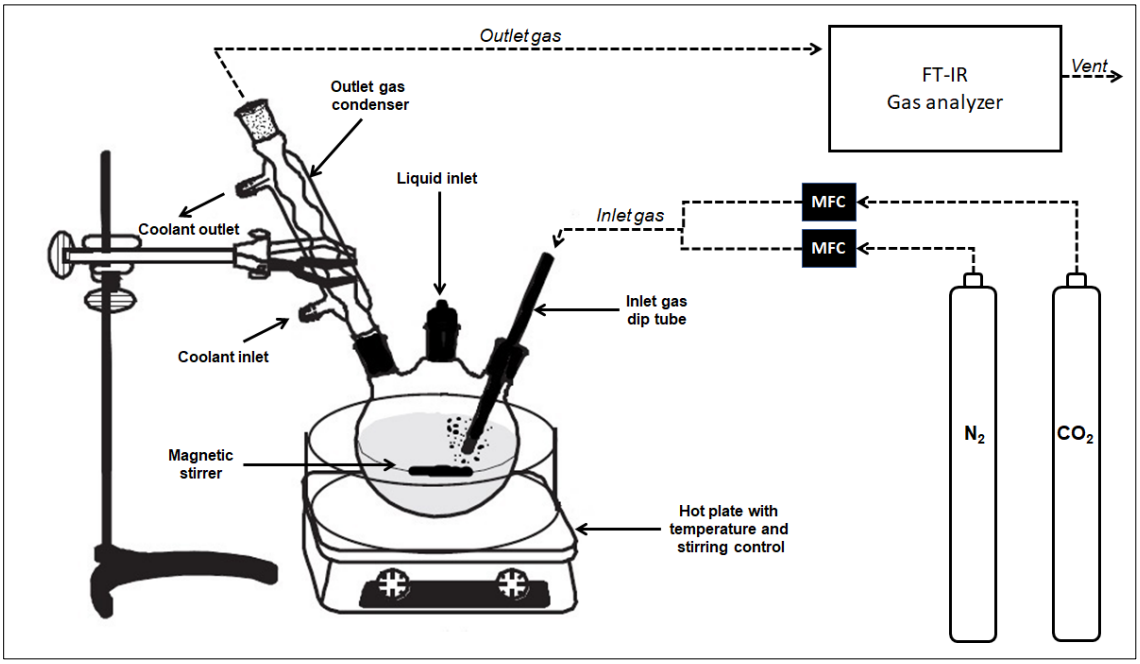

Figure 9: CO_2 absorption/desorption experimental setup

Different reaction conditions were chosen based on the experiment objective. The gas feed (either N_2 or CO_2) was introduced to the reactor through a dip tube (¼ in opening) inserted into the first neck of the flask with flow rates varied in the range from 0.05 – 0.2 liter/h. The middle neck was fitted with a glass stopper and was used to introduce the liquid solution to start the

absorption or the desorption experiment. The third flask neck was used as a gas outlet and was attached to a glass condenser. The amount of liquid MEA solutions were between 35 – 200 ml. All absorption experiments were conducted at 20 ^{o}C temperature and a stirring rate of 700 rpm. Desorption experiments were carried out at temperatures ranging between 80 – 82 ^{o}C with a similar stirring rate of 700 rpm. The glass condenser was used to condense the vapors in the outlet gas of the reactor. A refrigerant chiller was used to circulate water through the glass condenser at a temperature of 6 ^{o}C. The non-condensable outlet gases from the reactor were sent to the FT-IR gas analyzer to measure the CO_2 content.

4.5 Experiment procedure and protocol

4.5.1 Absorption experiments

In a typical experiment, the three-neck flask reactor was be loaded with the required amount of feed and immersed into the water bath which was placed over the heating plate with the magnetic stirrer. The temperature of the heating bath was controlled by manually manipulating the heating input to the plate. During the absorption step of MEA, 99.99 vol% CO_2 feed gas was continuously introduced to the empty reactor though a wide opening dip tube at a rate of 1 Liter/min/Liter solution until the outlet concentration measured by FT-IR stabilized at the feed composition value. A feed dip tube was purposely chosen over a gas sparger to reduce the gas residence time and allow faster CO_2 breakthrough. This is because our study only targeted the experimental stage where MEA had the highest CO_2 capture activity. Once both the water bath temperature (20 ^{o}C) and the outlet gas composition were stabilized, the absorption experiment started by charging the MEA solution into the reactor. As a measure to ensure that only the experimental region with high MEA activity was targeted, the absorption step was conducted until

CO_2 breakthrough concentration reached 12% of the feed gas concentration. One exception to this protocol was when determining the absorption capacity of MEA, where the experiment was run until the outlet CO_2 concentration stabilized at a constant value for few minutes.

4.5.2 Desorption experiments

During MEA regeneration step where heating was required, pre-determined amount of the solution was charges to the reactor once the water bath temperature had equilibrated at the desired value of 80-82 ^oC at a specific electric heater input. Ultra-high purity nitrogen at a flow of 0.3 – 0.4 L/min was used as a sweeping gas. The desorption time was set at 40 minutes for all liquid samples after which the reactor was quenched in a cold-water bath to stop the experiment. For the experiments that attempted to precipitate dissolved CO_2 through the reaction with calcium ions, different solid precursors were dispersed in the saturated MEA solutions prior to either the absorption or desorption experiments. Because one of the main objectives of this study was to enhance CO_2 desorption from MEA solutions, the regeneration improvements were linked to the increase in CO_2 desorption or precipitation in treated MEA compared with untreated MEA at similar regeneration conditions. Table 2 summarizes the conditions for the absorption and desorption experiments.

Table 2: Absorption and desorption experiment conditions

Parameter	**Absorption Experiments**	**Desorption Experiments**
Feed gas	High purity Carbon dioxide	Ultra-high purity N_2
Gas concentration [%]	100 (or 13% in N_2)	100
Gas flow rate [L/min]	0.04 - 0.12	0.1-0.3
Stirring rate [rpm]	700	700
Temperature [^oC]	20	80-82
Experiment ending criteria	CO_2 outlet concentration reaches 12.5%	40 minutes duration

4.6 Calculating CO_2 absorption capacity of MEA

The loading capacity of the tested solution was calculated by the summation of the difference in instantaneous molar flows (the initial gas molar flow minus the average outlet molar flow between every two measurements) multiplied by the sampling time difference between every two data measurements.

$$N_{CO_2,Li} = \sum_1^n \left\{ V \left[1 - \frac{(x_n + x_{(n-1)})}{2} \right] \times \frac{P\,\Delta t_n}{R\,T} \right\} \quad (19)$$

In equation 19, $N_{CO_2,Li}$ is the moles of CO_2 absorbed in MEA, V is the volumetric flow rate of the inlet gas, x is the CO_2 molar fraction in the outlet gas, P is the system's gas pressure, R is the gas constant and Δt is the measurement time difference for every step n.

4.7 Modeling the effect of CO_2 mineralization using Aspen Plus

To test the effect of adding different calcium precursors on the absorption and desorption processes of MEA solutions, a simplified process was simulated using Aspen Plus® with eNRTL thermodynamic property package. The model was run using ASPENPCD, AQUEOUS, SOLIDS, INRGANIC, and PURGE26 as property data banks. One primary goal of the model was to study the thermal regeneration of MEA and compares it with the mineralization-coupled regeneration by looking at the streams' composition, pH, duty for CO_2 removal and the re-absorption ability. The model was comprised of a CO_2 absorber with 20 equilibrium stages and a flash drum with variable heating duty to determine the energy required to desorb CO_2 to the gas phase. The MEA and flue gas streams were fed to the top and bottom stages of the absorber, respectively, and the rich MEA

solution was then fed to flash drum. Table 3 summarizes the properties and compositions of the different streams of the base case. As can be noted from table 3, the lean MEA was chosen to have a loading of 0.33 mol CO_2/mol MEA to mimic a composition of partially regenerated MEA stream which could be observed in real industrial processes.

Table 3: MEA and flue gas stream properties used in Aspen Plus simulation.

Property	Unit	Flow gas	Lean MEA	Treated gas	Rich MEA
Temperature	^oC	40.0	40.0	45.2	66.4
Pressure	bar	1.0	1.0	1.0	1.0
H_2O	kmol/hr	0.0	10.6	0.2	10.3
N_2	kmol/hr	3.4	0.0	3.4	0.0
CO_2	kmol/hr	0.5	0.0	0.0	0.0
MEA	kmol/hr	0.0	1.0	0.0	0.1
MEA^+	kmol/hr	0.0	1.0	0.0	1.5
$MEACOO^-$	kmol/hr	0.0	1.0	0.0	1.4
HCO_3^-	kmol/hr	0.0	0.0	0.0	0.1
CO_3^{--}	kmol/hr	0.0	0.0	0.0	0.0
Mass Flows	kg/hr	115.9	418.9	98.2	436.6
pH at 25 ^oC		-	9.9	-	8.6

4.8 Analysis of the mass transfer enhancement caused by solids in solution

Because the CO_2 desorption process involves the transfer of the solute across two contacting phases; namely the liquid MEA solution and the stripping N_2 gas, it was appropriate to use the two-film theory which was initially suggested by Whitman (Whitman 1962). The two-film theory mainly assumes that the diffusion rate is controlled by the diffusion within the gas and liquid phases while there is no transfer resistance across the gas-liquid interphase. In our analysis for the desorption process, the transfer of the solute (CO_2) happens through three main steps: (1) the transfer of CO_2 from the bulk liquid of MEA solution, (2) the transfer of CO_2 across the gas-

liquid interface, and (3) the transfer of CO_2 gas to the bulk of the N_2 stripping gas. As can be seen in the below analysis, the mass transfer enhancement was quantified by measuring the increase in the effective gas-liquid interfacial area.

Since the absorption and desorption processes are considered reversible, we start by writing the CO_2 mole balance between the two phases as in equation 20.

$$N_{CO_2,Li} - N_{CO_2,G} = N_{CO_2,Lf} \tag{20}$$

$$N_{CO_2,G} = \sum_1^n \left\{ \frac{V_{N_2}\left[\frac{x_n + x_{n+1}}{2}\right]}{\left[1 - \frac{x_n + x_{n+1}}{2}\right]} \times \frac{P\,\Delta t_n}{R\,T} \right\} \tag{21}$$

Where $N_{CO_2,Li}$ is the total number of CO_2 moles absorbed as defined in equation 19, $N_{CO_2,G}$ is the total number of CO_2 moles desorbed in the N_2 stripping gas as defined in equation 21, $N_{CO_2,Li}$ is the total number of CO_2 moles remaining in the MEA solution, V_{N_2} is the volumetric flow rate of the N_2 stripping gas during desorption, , x is the CO_2 molar fraction in the stripping gas, P is the system's gas pressure, R is the gas constant and Δt is the measurement time difference for every step n.

According to the two-film theory, the molar flux (J_{CO_2}) of a solute transporting across a two-phase interface can be represented by equations 22 and 23.

$$J_{CO_2} = k_L(C_{CO_2} - {C_{CO_2}}^i) \tag{22}$$

$$J_{CO_2} = k_G({P_{CO_2}}^i - P_{CO_2}) \tag{23}$$

Where C_{CO_2} is the concentration of CO_2 in the bulk liquid phase, P_{CO_2} is its partial pressure in the bulk gas phase and the super script i indicates the interface concentration or the partial

pressure. k_L and k_G are the convective liquid and gas mass transfer coefficients, respectively. Because of the difficulty to measure the concentration and the partial pressure at the liquid-gas interface, it's more convenient to define the flux in terms of the overall driving force which includes the resistances of both phases in terms of the partial pressure driving force as in equation (24).

$$J_{CO_2} = K_G(P_{CO_2}{}^{*} - P_{CO_2}) \tag{24}$$

Where $P_{CO_2}{}^{*}$ is the partial pressure of CO_2 in equilibrium with its concentration in the bulk liquid phase and K_G is the overall mass transfer coefficient based on the pressure driving force. At low solution concentrations, Henry's law can be applied to relate the solution concentrations to the equilibrium partial pressures as in equations 25 – 27 where m is Henry's constant.

$$P_{CO_2}{}^{i} = m\, C_{CO_2}{}^{i} \tag{25}$$

$$P_{CO_2}{}^{*} = m\, C_{CO_2} \tag{26}$$

$$P_{CO_2} = m\, C_{CO_2}{}^{*} \tag{27}$$

By using the above relations and manipulating the results, the overall mass transfer resistance can be written as in equation 28.

$$\frac{1}{K_G} = \frac{m}{k_L} + \frac{1}{k_G} \tag{28}$$

Because of the finite gas bubble size caused by the use of a very fine gas sparger, the diffusion from the liquid-gas interface to the gas bulk becomes much faster than the transfer from the liquid to the interface. Therefore, the gas side mass transfer resistance can be ignored (T. Wang

et al. 2016). By substituting for the overall mass transfer coefficient and writing the flux in terms of measurable variables, equation 29 can be obtained.

$$J_{CO_2} = k_L \left[C_{CO_2} - \left(\frac{P_{CO_2}}{m} \right) \right] \tag{29}$$

Then, the interfacial contact area between the liquid and gas phases can be written in terms of desorption molar flux as in equation 30 where n_{CO_2} is the molar desorption rate of CO_2.

$$A = \frac{n_{CO_2}}{J_{CO_2}} = \frac{n_{CO_2}}{k_L \left[C_{CO_2} - \left(\frac{P_{CO_2}}{m} \right) \right]} \tag{30}$$

where $n_{CO_2} = \frac{N_{CO_2,G}}{\Delta t_n}$

Because the objective of the study was to test for the desorption/absorption mass transfer enhancement caused by the increase in the interfacial contact area between the liquid and gas phases, the ratio of the area increase was used to signify this enhancement as defined in equation 31.

$$R = \frac{A_{solids}}{A_{no\ solids}} = \frac{\sum_0^s \left\{ \frac{n_{CO_2}}{k_L \left(m\, C_{CO_2} - P_{CO_2} \right)} \right\}_{solids}}{\sum_0^s \left\{ \frac{n_{CO_2}}{k_L \left(m\, C_{CO_2} - P_{CO_2} \right)} \right\}_{no\ solids}} \tag{31}$$

Although it is known that the convective liquid mass transfer coefficient depends on several factors such as the CO_2 loading, the temperature, and the viscosity of the liquid (Darde et al. 2011), the k_L terms for the solid-loaded and solid free solutions were assumed to be equal for simplicity and they cancel out in equation 31. This assumption was considered reasonable baring that some studies report the ratios of the liquid mass transfer coefficient as close to unity (T. Wang et al. 2015). In equation 31, C_{CO_2} represents the bulk concentration of CO_2 in the liquid phase and was

calculated by subtracting the desorbed CO_2 from the initial solution loading. m is Henry's constant evaluated at the regeneration temperature (80 ^oC) and was calculated using literature relations for 30% MEA solutions at 80 ^oC (Dang and Rochelle 2003). P_{CO_2} is the partial pressure of CO_2 in the bulk gas phase and was taken as half the partial pressure of CO_2 in the outlet gas (as average pressure during bubble desorption). Because the interfacial area was changing along the duration of the experiments, the average values across determined measurements "*s*" was taken in equation 29. Table 4 summarizes experimental parameters and the equations used to calculate the interfacial gas-liquid areas for the tested solutions.

Table 4: Parameters and additional equations used to calculate the interfacial gas-liquid area for the tested solutions.

Parameter	Value	Note
Desorption temperature (^oC)	80	
Desorption pressure (atm)	1	
Stripping N_2 flow rate (L/min)	0.2	Using ultrahigh purity N_2 gas
Desorption duration (min)	30	
Gas concentration measurement frequency time (min)	0.25 – 0.30	
Aqueous MEA solution concentration (vol%)	22	
MEA solution volume for desorption (L)	0.05	
MEA solution loading before desorption (mol CO_2/mol MEA)	0.42 - 0.43	
MEA solution loading after desorption (mol CO_2/mol MEA)	0.28	
CO_2 desorption rate (mol/min)	$n_{CO_2} = \frac{N_{CO_2,G}}{\Delta t_n}$	
CO_2 concentration in the Bulk MEA solution (mol/L)	$C_{CO_2} = \frac{[Remaining\ CO2\ in\ solution]}{[Solution\ volume]} = \frac{N_{CO_2,Lf}}{0.05}$	
CO_2 partial pressure in the bulk gas phase (atm)	$P_{CO_2} = \frac{[partial\ pressure\ of\ CO2\ in\ the\ outlet\ gas]}{2}$	
Interfacial gas-liquid area ratio	$R = \frac{\sum_0^s \left\{\frac{n_{CO_2}}{(m\,C_{CO_2} - P_{CO_2})}\right\}_{solids}}{\sum_0^s \left\{\frac{n_{CO_2}}{(m\,C_{CO_2} - P_{CO_2})}\right\}_{no\ solids}}$	This was calculated by the summation of the terms and taking the ratio for three different time segments (0-5, 5-10, and 10-15 min). See section 5.2.6
Henry's constant (atm.L/mol)	$m = 95.7\ at\ 80^oC$	Calculated from (Dang and Rochelle 2003)
Liquid phase mass transfer coefficient (mol./(min.m^2.atm)	$k_L = 12$	Estimated for solid-free MEA solution at 40 ^oC (Darde et al. 2011)

Another way of assessing transport enhancement by the addition of solid particles, was to introduce a quantity named the *Enhancement Factor* (E). Defined in equation 32, the enhancement factor is the ratio of the maximum CO_2 gaseous desorption (or absorption) rate from (or into) MEA with solid particles $N_{max\text{-}solids}$ (mol/min) to the maximum gaseous desorption (or absorption) rate without solids N_{max} (mol/min).

$$E = \frac{N_{max-solids}}{N_{max}} \tag{32}$$

5 Results and discussion

5.1 Quantifying MEA absorption capacity

This section provides the method for quantifying the absorption capacity of MEA and compares it with the values obtained from literature. 22 vol% MEA was used as the default amine solution in all further experiments. In a typical experiment, 50 ml volume of MEA solution placed in a constant temperature water bath at 20 ^oC was bubbled with 100% CO_2 gas at a flow rate of around 0.12 Liter/min until the CO_2 concentration stabilized at an equilibrium value for around 10 minutes. The absorption capacity was calculated from the breakthrough curve shown in figure 10 using equation 19.

The experiment was repeated several times to ensure consistency and repeatability of results. Measured loading capacities of CO_2 in MEA were in the range between 0.46 – 4.8 mol CO_2/mol MEA which were in close agreement with the stoichiometric value of 0.5 mol/mol. These

values were also within experimental results reported in literature which can range between 0.45 – 0.8 mol/mol depending on factors such as MEA concentration, mixing rate, feed composition and reaction temperature (Huertas et al. 2015; Kim et al. 2013).

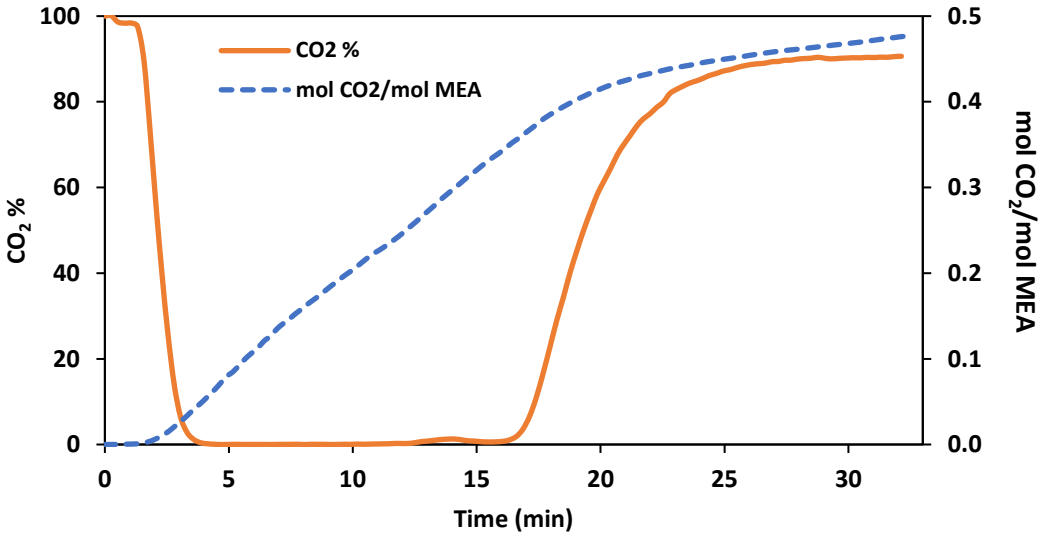

Figure 10: breakthrough curve from absorbing pure CO_2 in 22 vol% MEA solution at 20 °C.

5.2 MEA desorption experiments

Because it is an essential objective of this study to effectively regenerate rich MEA to a loading that is well below 0.3 mol CO_2/mol MEA (where carbamate ions are most stable and MEA has highest activity (Lv et al. 2015)), MEA solutions were loaded with CO_2 to within the 0.27 – 0.4 mol/mol range. The CO_2 breakthrough curve is shown in figure 11 and the experimentally relevant region of CO_2 loading is highlighted. Because in our study the targeted absorption capacity (in mol CO_2/mol MEA) was limited to the range where MEA solution was most active

towards absorption with almost 100% CO_2 capture, the absorption experiment was stopped when the breakthrough concentration reached 12.5%. At these conditions, the saturated solutions had CO_2 loadings in the range of 0.38 – 0.43 mol/mol.

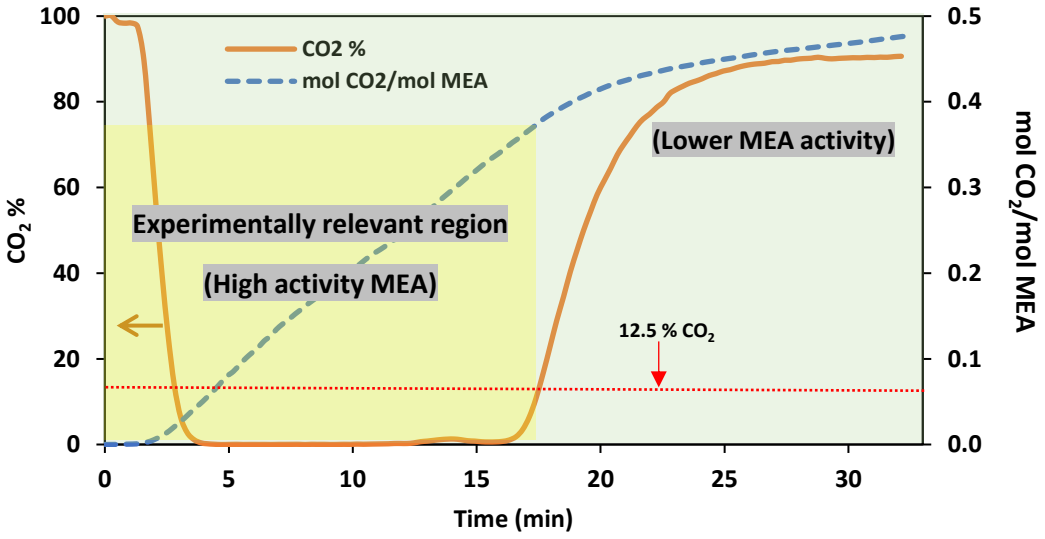

Figure 11: Breakthrough curve of absorbing pure CO_2 gas in 22 vol.% MEA solution at 20 ^oC with the experimentally relevant region highlighted

5.2.1 MEA desorption using $Ca(OH)_2$

Several experiments were performed to evaluate the influence of adding $Ca(OH)_2$ into saturated MEA before stripping. 200 ml of fresh MEA solution was bubbled with CO_2 according to the protocol mentioned earlier and then the saturated amine solution was divided into three equal batches of 50 ml. Then, each batch of 50 ml solution was mixed with $Ca(OH)_2$ solid loadings of 0, 0.1, 1.0, and 5.0 g before stripping the solution at 80 ^oC for 40 min. The resulted CO_2 saturation curves are shown in figure 12. From the results, it is clear that adding $Ca(OH)_2$ solids gradually

reduced the amount of desorbed CO_2 during MEA regeneration until the point where no CO_2 desorption was observed when 5.0 g of $Ca(OH)_2$ (stoichiometric amount to CO_2 in solution) were added. This is expected considering that some of the absorbed CO_2 would readily precipitate as $CaCO_3$ through reaction 18 and as confirmed by other similar studies (Ji et al. 2018).

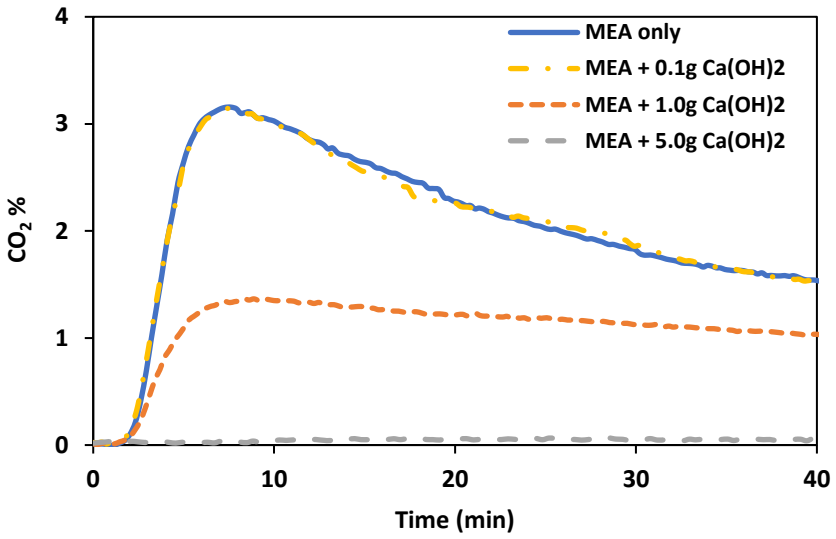

Figure 12: MEA regeneration by adding different amounts of $Ca(OH)_2$ at 80 ^oC

TGA analysis of the collected solids from adding 1.0 g of $Ca(OH)_2$ showed that only 0.63% the sample's weight loss occurred before 600 ^oC then a sharp weight loss occurred in the temperature range from 650 – 900 ^oC. The ratio of the remaining solid weight to the sample weight at 600 ^oC was 0.56 g/g which exactly matched the mass ratio of pure CaO to $CaCO_3$ indicating that almost all of the analyzed solid was calcium carbonate decomposing to calcium oxide. Figure 13 shows the TGA isotherm of the solid weight loss. Aside from capturing some of the CO_2 in carbonate form, the dispersed (or generated) solid particles were expected to enhance the desorption mass transfer allowing more CO_2 to desorb in the gas phase (T. Wang et al. 2016; Jiang

et al. 2014; W. Yu et al. 2019). This was evident by observing that adding 0.1 g of $Ca(OH)_2$ desorbs similar amount of gaseous CO_2 while precipitating some CO_2 as $CaCO_3$. Table 5 shows the calculated desorption amounts in mol CO_2/mol MEA and figure 14 shows the solution's pH value after every step.

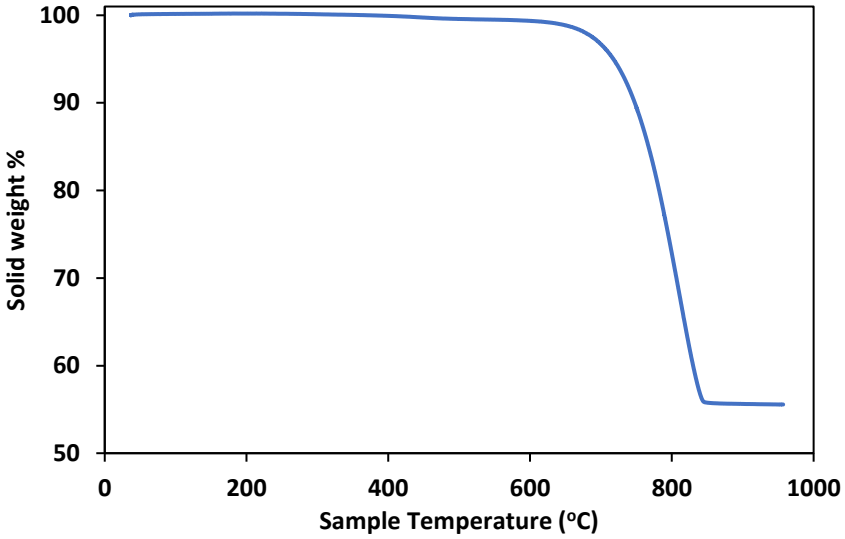

Figure 13: TGA analysis of the solids generated from mineralizing CO_2 using $Ca(OH)_2$

Table 5: Experimental results of regenerating MEA with $Ca(OH)_2$ at 80 °C

Sample	Initial CO_2 loading	Desorption *(Gas)*	Desorption *(Solid)*	CO_2 removed	Collected solids	Final CO_2 loading
	[mol CO_2/mol MEA]			*[%]*	*[g]*	*[mol CO_2/mol MEA]*
MEA	**0.381**	0.072	-	18.9	-	**0.309**
MEA + 0.1 g $Ca(OH)_2$	**0.381**	0.072	0.006	20.6	0.113	**0.302**
MEA + 1.0 g $Ca(OH)_2$	**0.381**	0.037	0.070	28.2	1.279	**0.274**
MEA + 5.0 g $Ca(OH)_2$	**0.381**	0.002	0.330	87.1	6.038	**0.049**

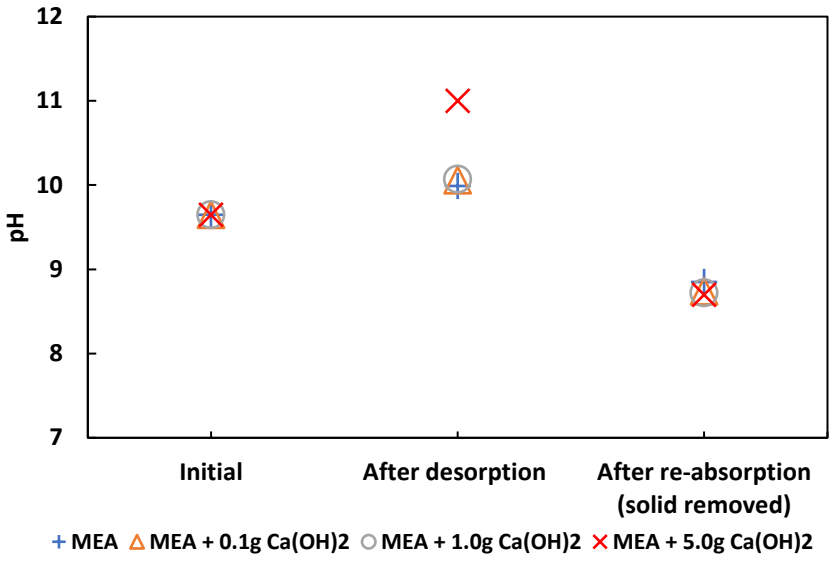

Figure 14: Saturated MEA pH change with the addition of $Ca(OH)_2$

After the first desorption experiment, all MEA solutions regenerated with 0 - 1.0 g of $Ca(OH)_2$ had almost the same pH value of 10. The only exception was MEA solution regenerated with 5.0 g $Ca(OH)_2$ which had a pH value of 11. This could be attributed to the higher regeneration extent within this sample causing the pH to be higher approaching the pH value of 12.8 for the fresh MEA.

The liquid MEA solutions before and after absorption/desorption steps were structurally compared using the liquid state FT-IR. Figure 15 shows the FT-IR vibration spectra for MEA solutions with different $Ca(OH)_2$ loadings. As can be seen in figure 15, the intensity of the carbamate, bicarbonate and carbonate peaks decreased significantly as more $Ca(OH)_2$ was added. Moreover, when the solid loading approached the stochiometric amount of CO_2 in the solution, the unprotonated MEA peak around 950 cm^{-1} started to evolve. Surprisingly, adding a

stoichiometric amount of $Ca(OH)_2$ while regenerating at 80 ^oC resulted in a solution that precisely matches the spectra of the fresh amine indicating the structural similarity of the two. As can be inferred from table 5, the calculated amounts of removed CO_2 in both gas and solid shows that around 87% of the captured CO_2 was removed by adding stoichiometric amount of $Ca(OH)_2$ and heating. It is clear that MEA regeneration by mineralization was greatly facilitated by only heating the solution to a low temperature of 80 ^oC for 40 min – a condition where only 18% of the absorbed CO_2 was removed thermally. Both the FT-IT and the CO_2 removal analysis shows a significant regeneration improvements with more than double the percent CO_2 reported by similar studies regenerating at 40 ^oC (Ji et al. 2018).

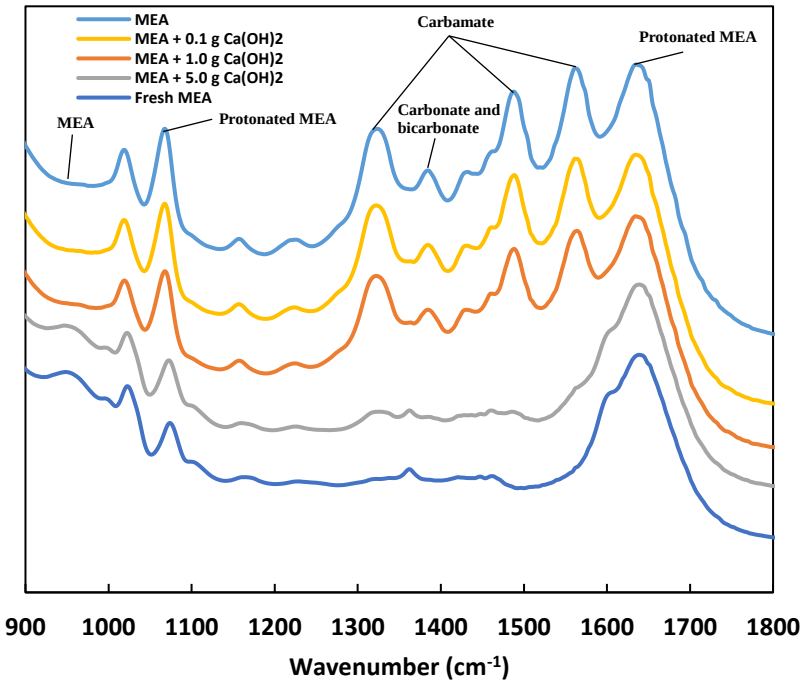

Figure 15: FT-IR spectra for MEA solutions regenerated with different amounts of $Ca(OH)_2$ at 80 ^oC for 40 min.

In order to decouple the thermal effect caused by heating at 80 ^oC from the carbonation reaction alone, a separate experiment was conducted to check the structural changes of saturated

MEA when $Ca(OH)_2$ was added in 3 equal amounts until reaching the stoichiometric CO_2 loading. Figure 16 shows the spectra when $Ca(OH)_2$ was added in different amounts to saturated MEA at 20 ^oC. It can be seen that adding $Ca(OH)_2$ greatly reduced the peak intensity of the protonated MEA to the level that almost matched the fresh amine. On the other hand, carbamate, carbonate, and bicarbonate peaks were reduced but to a much smaller extent. It seems that CO_2 mineralization with calcium wouldn't proceed as expected when the solutions were at lower temperatures due to the high stability of carbamate ions (Ji et al. 2018). This is particularly true considering that adding $Ca(OH)_2$ would greatly increases the alkalinity of the solution to the point where it becomes insoluble and remains as solid. This proves that neither heating nor CO_2 mineralization alone could effectively regenerate MEA. It is intuitive to realize that liquid CO_2 mineralization in saturated MEA requires activation by heating up the solution to both facilitate the generation of carbonates and increase the solubility of calcium hydroxide.

Figure 17 shows the pH variation in saturated and fresh MEA solutions when incremental amounts of $Ca(OH)_2$ were added until reaching a stoichiometric ratio of 1 mol Ca^{2+}/mol CO_2. As can be seen in figure 17, the pH value of the fresh MEA solution stabilized at 12.8 upon the first solid addition and maintained this value even with subsequent solid additions. This proves that the solution at this pH has already reached the solubility limit of $Ca(OH)_2$ preventing further dissolution to free Ca^{2+} ions.

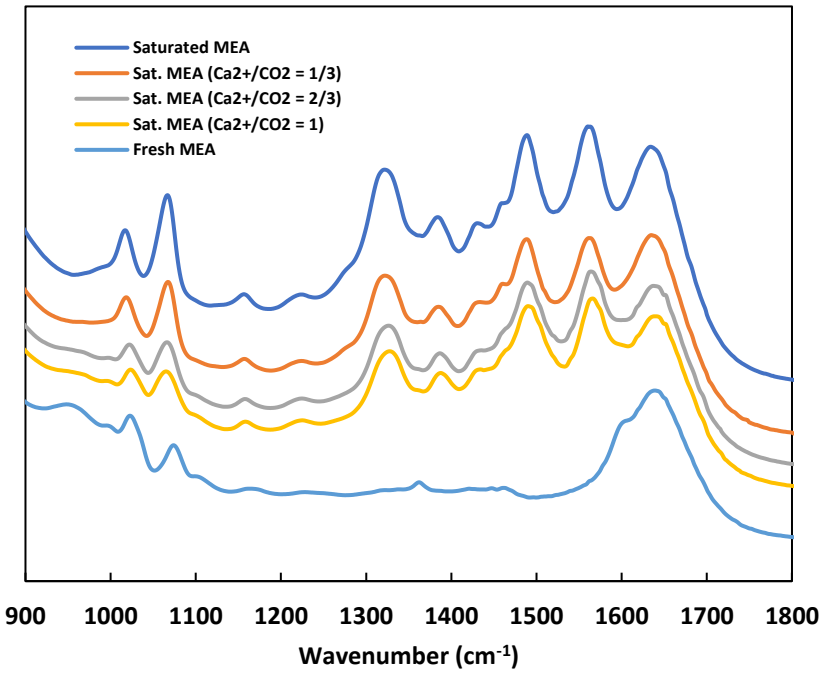

Figure 16: Spectra of Saturated MEA regenerated with different amounts of $Ca(OH)_2$ at 20 ^oC for 15 min.

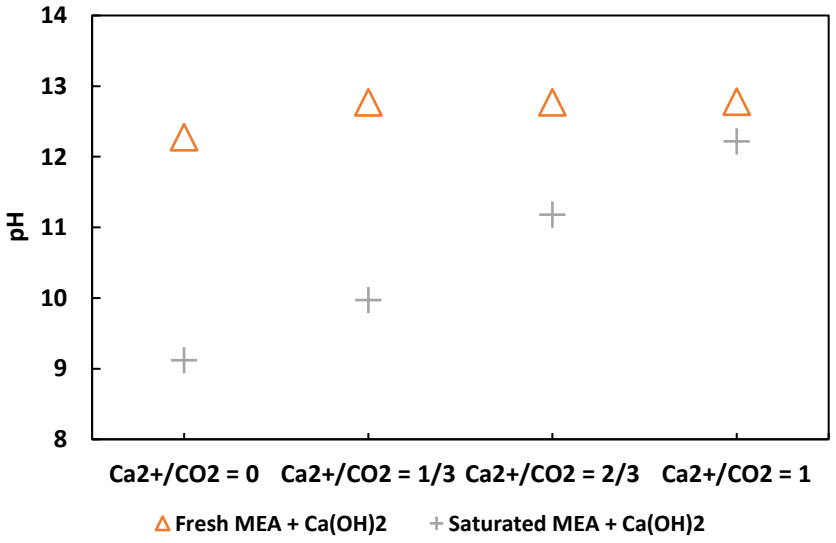

Figure 17: influence of adding incremental amounts of $Ca(OH)_2$ on the pH of saturated and fresh MEA.

To further confirm the regeneration of MEA through CO_2 mineralization by calcium, all MEA solution were brought through a second absorption experiment after removing all precipitated solids. Figure 18 shows the breakthrough curve for the second absorption experiment for the four solutions. It is important to point out that because each solution had a different absorption isotherm starting/ending point (due to differences in regeneration extent), a relative comparison was not used. Instead, absolute absorption amounts are shown in figure 18. It's clear that all MEA solutions regenerated by mixing with $Ca(OH)_2$ had higher CO_2 re-absorption quantities proportional to the solid amounts added. This suggests that calcium was reacting with CO_3^{2-} causing an equilibrium shift in reaction 12 that resulted in converting carbamate to bicarbonate and availing more MEA. Moreover, the similarity in pH values of all MEA solutions after the second absorption (figure 14) was one way to indicate comparable chemical identity (in terms of free OH^- ions) across all solutions.

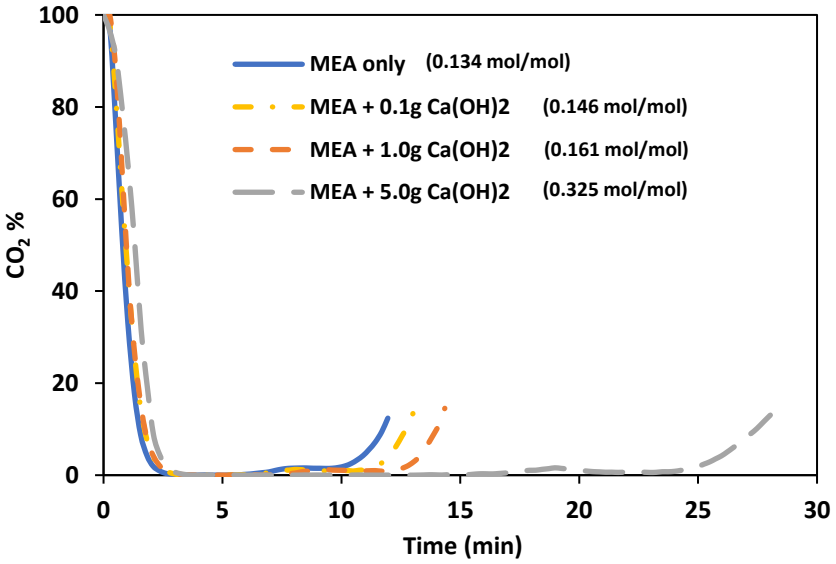

Figure 18: Breakthrough curves for the second absorption (at 20 °C) of four MEA solutions after regeneration with $Ca(OH)_2$ and removal of solids.

5.2.2 MEA desorption using $CaCl_2$

Analogous to the $Ca(OH)_2$ study, the influence of adding $CaCl_2$ as a calcium precursor has been studied using similar batches of 50 ml of saturated MEA loaded with 0, 0.1, 1.0 and 8.4 g of salt. Similarly, the highest loading of 8.4 g corresponding to the stoichiometric amount to balance CO_2 in solution. Using the same regeneration conditions of 80 ^oC and 40 min, the desorption isotherms for the four MEA solutions are shown in figure 19.

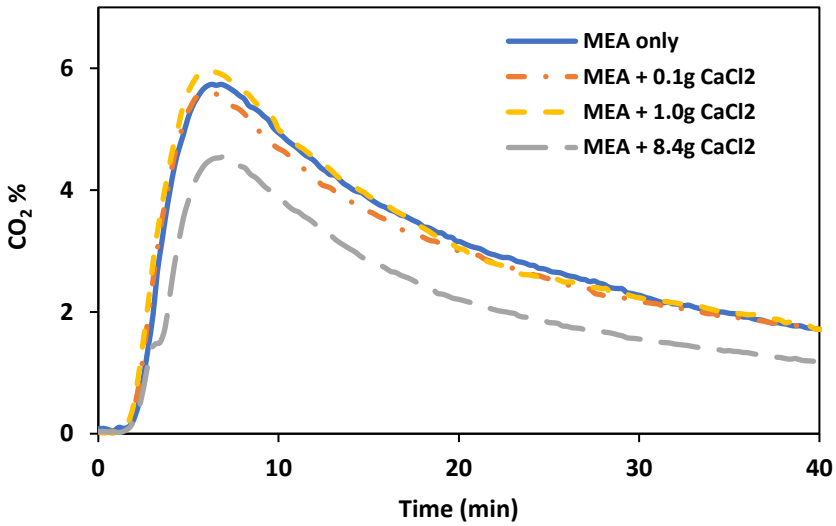

Figure 19: Desorption isotherms for MEA solutions regenerated with different amount of $CaCl_2$ at 80 ^oC for 40 min.

As can be inferred from figure 19 and table 6, adding $CaCl_2$ didn't cease the release of gaseous CO_2 from saturated MEA solutions during stripping even when a stoichiometric amount of calcium was added. Instead, almost similar amounts of CO_2 were released when adding 0.1 and 1.0 g of salt with slightly less amount when 8.4 g salt was added. Along with the gaseous release

of CO_2, white solids started to form as the regeneration experiment proceeded. It is important to note that upon mixing and dissolving $CaCl_2$ in saturated MEA at room temperature before loading the solution into the reactor, the solution didn't seem to visibly form solid particles. The precipitation process was observed to be much slower at room temperature compared to when the solution was heated to 80 ^oC. The solids that precipitated during regeneration of MEA were expected to be $CaCO_3$ as proven by XRD analysis done by similar studies using $CaCl_2$ at 40 ^oC. Indeed, the TGA results in figure 20 for the solid formed by the addition of 1.0g $CaCl_2$ indicated that 1.7% of the sample decomposed below 600 ^oC. The ratio of the remaining solid weight above 950 ^oC to the sample weight at 600 ^oC was 0.56 g/g which was also matching the mass ratio of pure CaO to $CaCO_3$.

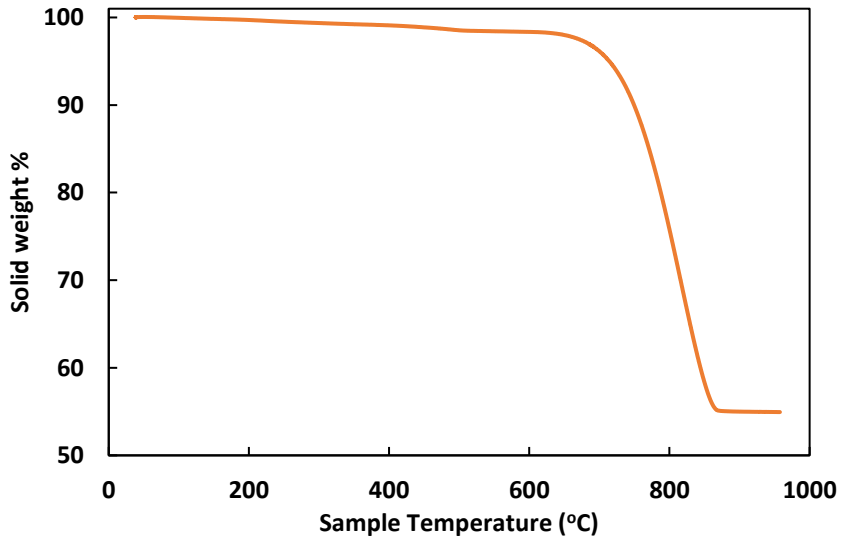

Figure 20: TGA analysis of the solids formed by mixing 1.0 g of $CaCl_2$ with saturated MEA at 80 ^oC for 40 min.

Table 6: Experimental results of regenerating MEA with $CaCl_2$ at 80 ^oC

Sample	Initial CO2 loading	Desorption *(Gas)*	Desorption *(Solid)*	CO_2 removed	Collected solids	Final CO2 loading
	[mol CO_2/mol MEA]			*[%]*	*[g]*	*[mol CO_2/mol MEA]*
MEA	**0.416**	0.109	0.000	26.3	-	**0.306**
MEA + 0.1 g $CaCl_2$	**0.416**	0.105	0.001	25.5	0.023	**0.309**
MEA + 1.0 g $CaCl_2$	**0.416**	0.111	0.033	34.6	0.611	**0.272**
MEA + 8.4 g $CaCl_2$	**0.416**	0.078	0.294	89.5	5.42	**0.044**

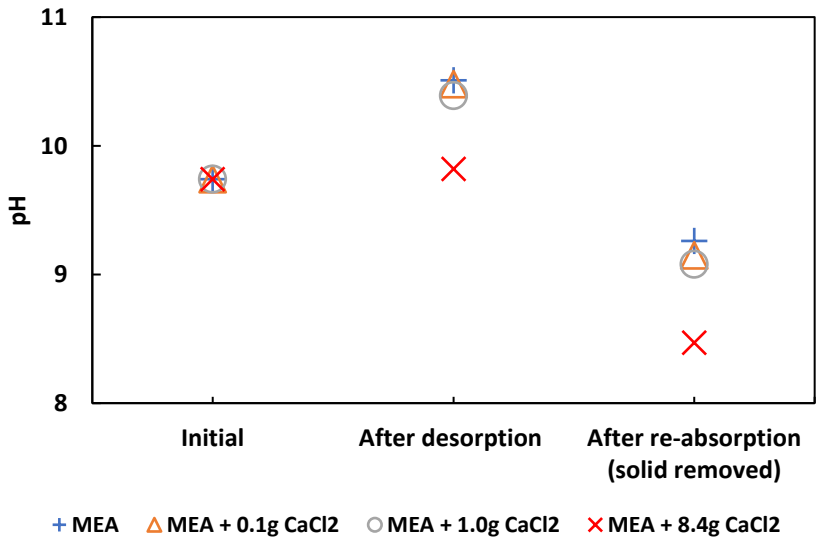

Figure 21: Saturated MEA pH change with the addition of $CaCl_2$

The FT-IR spectra for the $CaCl_2$-loaded and unloaded MEA solutions are shown in figure 22. As more $CaCl_2$ was added to the saturated MEA, the peaks corresponding to carbamate decreased accordingly. The addition of a stoichiometric amount of salt significantly reduced the carbamate, carbonate and bicarbonate peak intensity compared to the thermally treated MEA

solution. In addition, there was a clear increase in the amount of protonated amine evident by the rise in the peak intensity around 1050 cm^{-1} wavenumber. Moreover, the absence of the broad peak near the 950 cm^{-1} wavenumber signifies the lack of regenerated MEA in all solutions. These results suggest that MEA or regenerated carbamate from reactions (20) and (21) might have converted to protonated amine upon releasing CO_2 as in reaction (22). This is expected especially when more free protons are present. The results in figure 21 shows that adding $CaCl_2$ to saturated MEA decreased the pH and this result agreed the previous studies reported (Kang et al. 2018; Arti et al. 2017). Such lower alkalinity could be responsible for shifting the equilibrium of reaction (22) in the forward direction and reaction (23) in the reverse direction resulting in a gaseous release of CO_2 and a limited generation of CO_3^{2+}, respectively. The latter effect as well as the reduced alkalinity could result in reduced precipitation of $CaCO_3$. Indeed, the yield of the precipitated solid indicates that only 71.5 mol% of the added calcium was converted to calcium carbonate. Yet, this conversion was much higher than the value of 26% reported by a similar study using a stoichiometric amount of $CaCl_2$ to regenerate MEA at 40 ^oC. The substantial improvement in precipitation suggests the importance of the thermal effect in driving the precipitation process.

Although regenerating MEA with $CaCl_2$ made less precipitation yield (71.5%) compared to $Ca(OH)_2$ (90%), the total CO_2 percent removal from both gas release and solid precipitation was found to increase proportionally with the added amount of salt. As can be inferred from table 5, adding a stochiometric amount of $CaCl_2$ resulted in a total CO_2 removal of 89.5% - a value that almost matches the removal efficiency by adding $Ca(OH)_2$. The main difference was that $CaCl_2$ balanced the decrease in precipitation by desorbing CO_2 as gas.

$$MEA\,COO^- + H_2O \leftrightarrow MEA + HCO_3^- \quad (20)$$

$$MEA\,COO^- + H_3O^+ \leftrightarrow MEA + CO_2 + H_2O \quad (21)$$

$$MEA + H_3O^+ \leftrightarrow MEA\,H^+ + H_2O \quad (22)$$

$$HCO_3^- + H_2O \leftrightarrow CO_3^{2-} + H_3O^+ \quad (23)$$

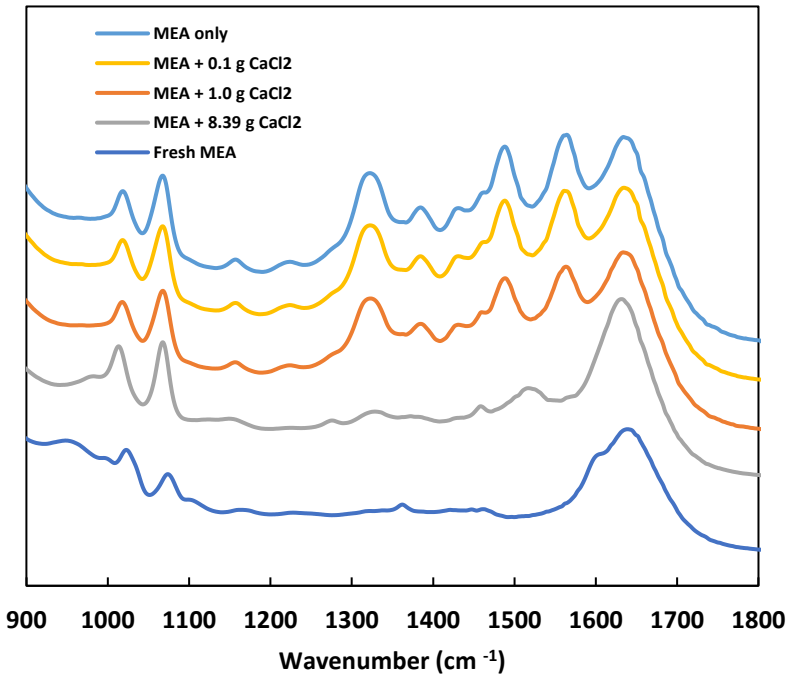

Figure 22: FT-IR spectra for MEA solutions regenerated with different amounts of $CaCl_2$ at 80 ^oC for 40 min

The effect of mixing different amounts of $CaCl_2$ in the saturated MEA solution at 20 ^oC has also been studied using FT-IR to structurally compare the solutions when the thermal effect was excluded. In this experiment $CaCl_2$ was added in three equal quantities until reaching the stoichiometric amount of CO_2 in solution. Figure 23 compares the FT-IR spectra of the treated and

untreated saturated MEA. Just like the thermally treated $CaCl_2$-MEA solution, adding $CaCl_2$ was seen to reduce the intensities of the peaks corresponding to carbamate, HCO_3^- and CO_3^{2-} with notable rise in the intensities of protonated MEA peaks. Unlike the case with the regeneration at a higher temperature of 80 ^oC, mixing the salt with saturated MEA at room temperature didn't spontaneously form precipitates. Instead, the salt was found to completely dissolve before solid precipitates started to evolve slowly. On the other hand, solid precipitation was observed to happen rapidly during the first few minutes of the desorption experiment at 80 ^oC. Figure 24 shows the pH changes of saturated and fresh MEA solutions when incremental amounts of $CaCl_2$ were added. The pH results further confirm the effect of Cl^- ions in reducing the pH even with the fresh MEA solution.

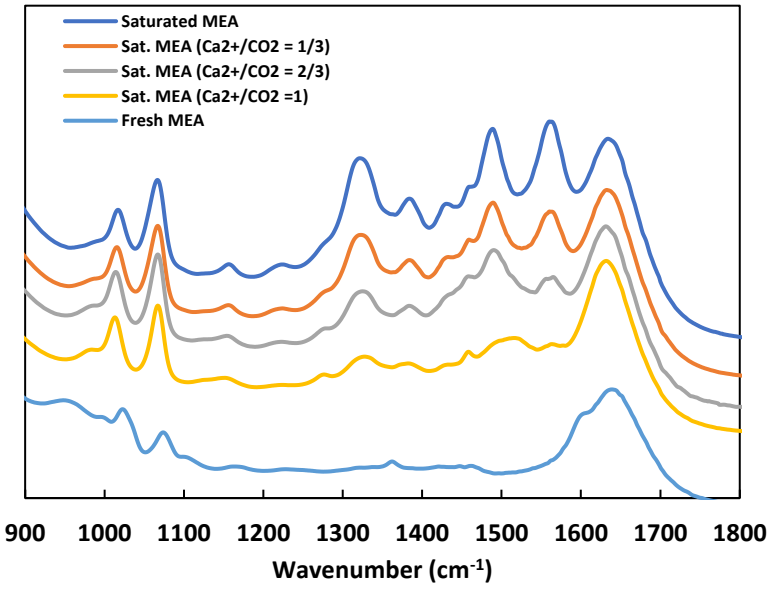

Figure 23: Spectra of Saturated MEA regenerated with different amounts of $CaCl_2$ at 20 ^oC for 15 min.

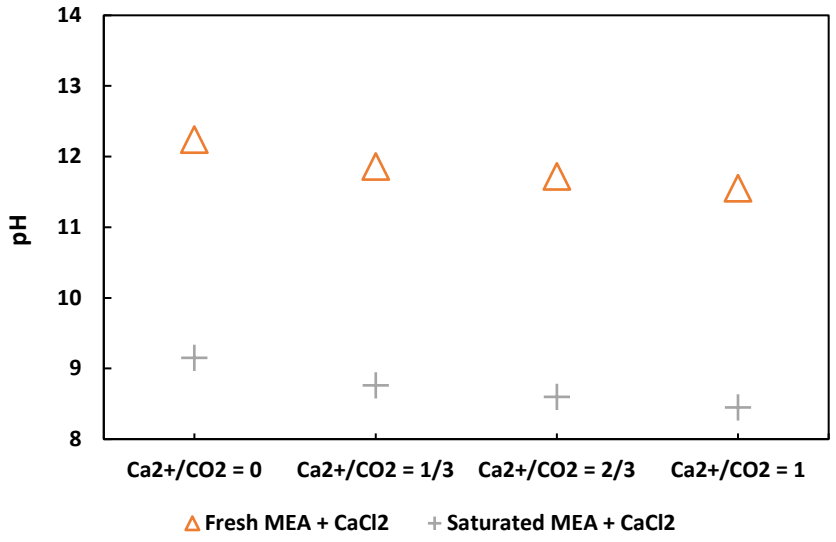

Figure 24: influence of adding incremental amounts of $CaCl_2$ on the pH of saturated and fresh MEA.

After conducting the desorption experiments and removing the generated solids, all the above solutions were subject to a second absorption experiment to measure the re-absorption ability. Figure 25 shows the breakthrough curves for the four solutions undergoing the second absorption. It can be observed that adding $CaCl_2$ generally reduced the reabsorption capacity of MEA with a notable decrease in the pH value of the CO_2-rich solution. The capacity decrease was much more pronounced in the case where a stoichiometric amount of salt was added. This can be explained by the presence of considerable amounts of protonated MEA in the lean solution (as indicated by FT-IR results) reducing the availability of free amine to absorb CO_2. Also, along with the presence of protonated MEA, some literature studies suggest the presence of chlorine bounded MEA species making such species inactive towards CO_2 absorption (Kang et al. 2018).

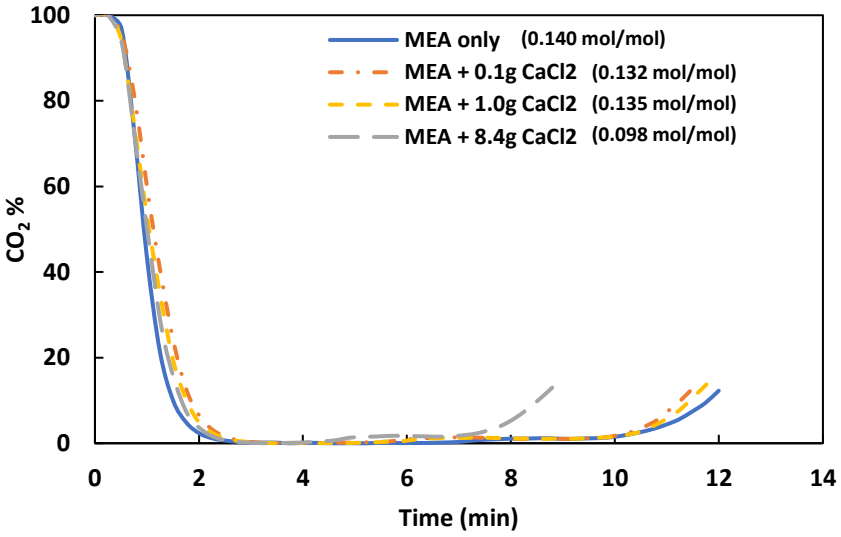

Figure 25: Breakthrough curves for the second absorption (at 20 °C) of four MEA solutions after regeneration with $CaCl_2$ and removal of solids.

5.2.3 MEA desorption using CaO

Calcium oxide solids obtained from marble were also tested for their ability to regenerate saturated amine by mineralization. Although their reaction with dissolved CO_2 to form $CaCO_3$ was expected to be chemically similar to that of $Ca(OH)_2$ (except that calcium hydroxide would produce one mole of water per mole hydroxide added), it was interesting to know how this calcium precursor would aid in the mineralization and the regeneration of MEA. In these experiments, three 50 ml solutions of equal CO_2 loadings were mixed with 0, 0.1 and 1.0 g of CaO solid particles with less than 80 mesh size. Then, each sample was subject to the same regeneration condition of 80 °C for 40 min. The resulted CO_2 saturation curves are shown in figure 26 and the calculated desorption amounts are shown in table 7. From the results, it is clear that adding $Ca(OH)_2$ solids gradually reduced the amount of desorbed CO_2 during MEA regeneration similar to what was observed with $Ca(OH)_2$. This was expected considering that some of the absorbed CO_2 would

readily precipitate as $CaCO_3$ through reaction (18) and as confirmed by other similar studies (Ji et al. 2018). Figure 28 shows that the pH did not significantly change with the addition of CaO. Although a stoichiometric amount of solid wasn't used, adding more amounts of CaO was expected to increase the pH and the extent of regeneration similar to $Ca(OH)_2$.

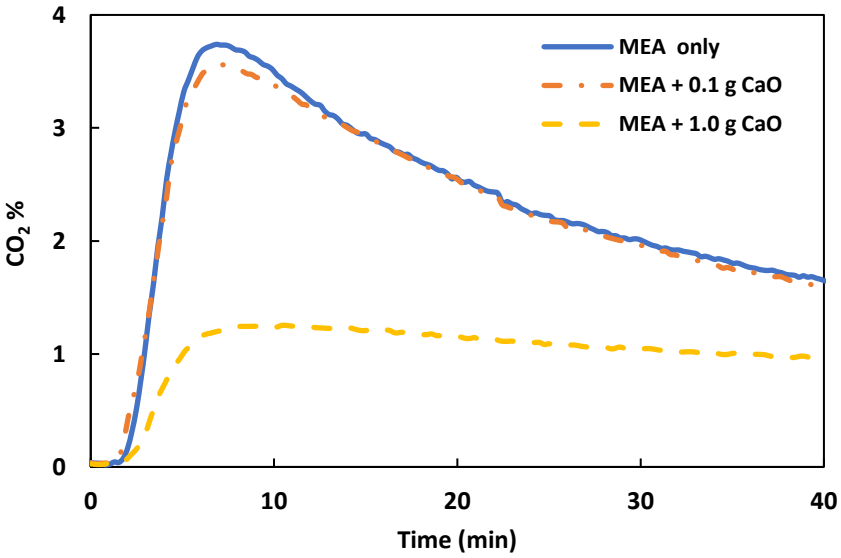

Figure 26: Desorption isotherms for MEA solutions regenerated with different amounts of CaO at 80 ^oC for 40 min.

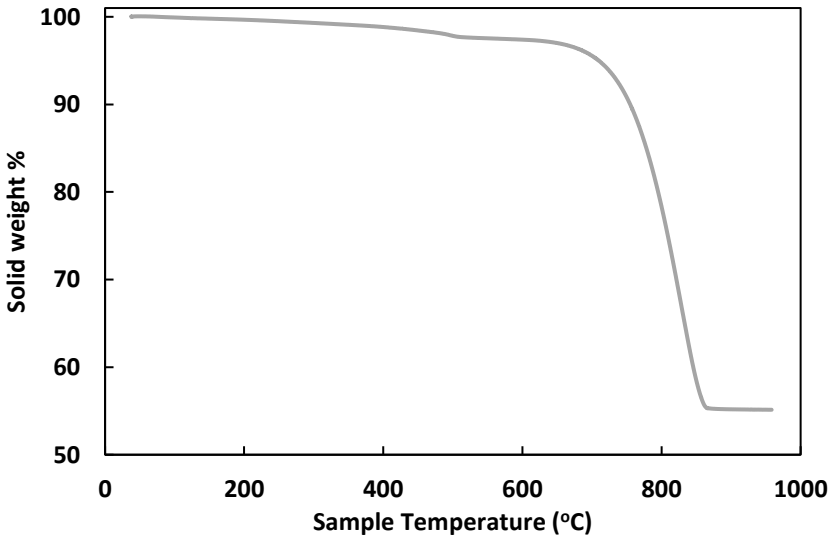

Figure 27: TGA analysis of the solids formed by mixing 1.0 g of CaO with saturated MEA at 80^oC for 40 min.

Table 7: Experimental results of regenerating MEA with CaO at 80 °C

Sample	Initial CO_2 loading	Desorption *(Gas)*	Desorption *(Solid)*	CO_2 removed	Collected solids	Final CO_2 loading
	[mol CO_2/mol MEA]			*[%]*	*[g]*	*[mol CO_2/mol MEA]*
MEA	0.395	0.086	0	21.6	-	0.31
MEA + CaO	0.395	0.084	0.0074	23	0.14	0.305
MEA + CaO	0.395	0.037	0.0883	31.6	1.67	0.271

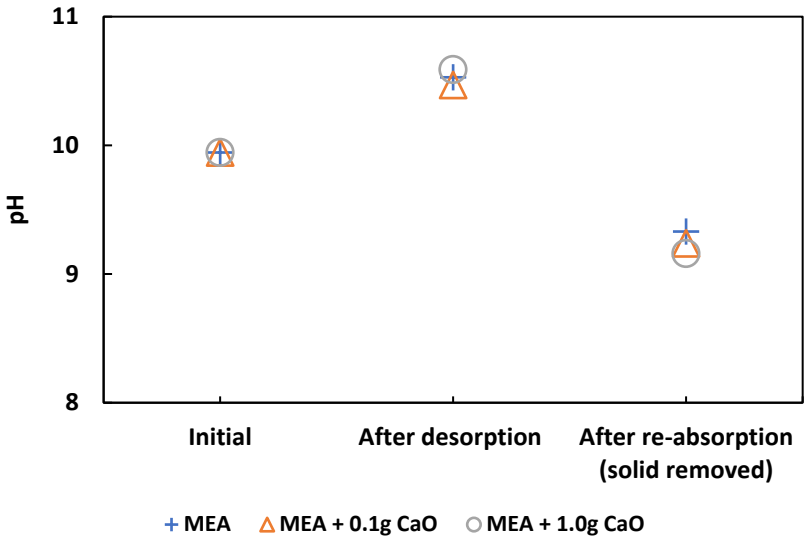

Figure 28: Saturated MEA pH change with the addition of CaO

The TGA results of the collected solids after the desorption experiment with 1.0 g CaO are shown in figure 27. The analysis indicates that 2.6 wt% of the sample decomposed before 600 °C. This could be attributed to the presence of chemically absorbed water (as calcium hydroxide). By applying similar mass ratio analysis, it was found that 97.4 wt% of the sample was $CaCO_3$. The minor difference in the purity of $CaCO_3$ solids generated by CaO to those formed from $Ca(OH)_2$ can be possibly explained by the difference in particle size in which the CaO particles were

expected to be bigger, and therefore, had more limited contact area with bicarbonate ions to make complete carbonation.

Figures 29 and 30 show the FT-IR spectra of the MEA solutions after treatment with CaO solids at 80 and 20 ^{o}C, respectively. From these results it was clear that CaO was capable of regenerating MEA in the same manner that $Ca(OH)_2$ did.

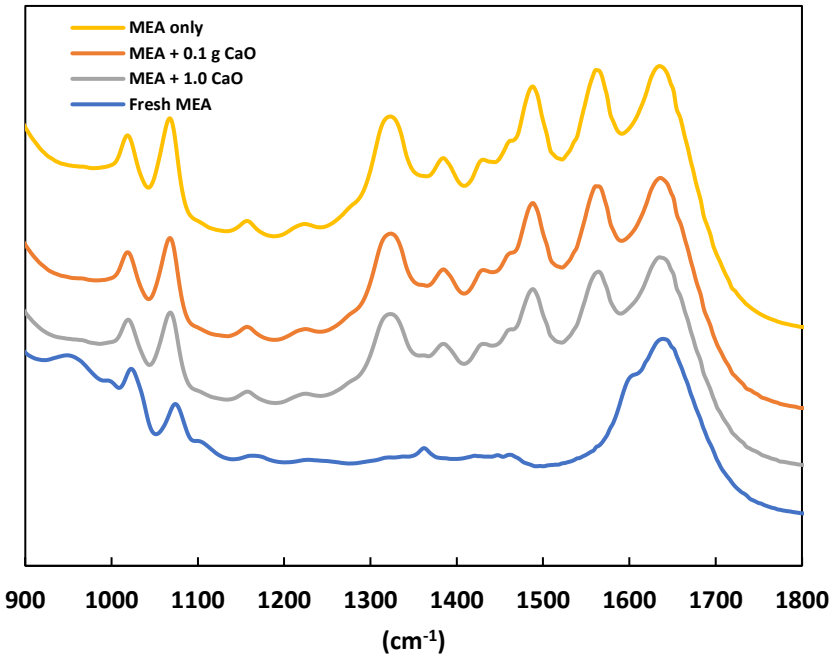

Figure 29: FT-IR analysis for MEA solutions treated with CaO at 80 ^{o}C

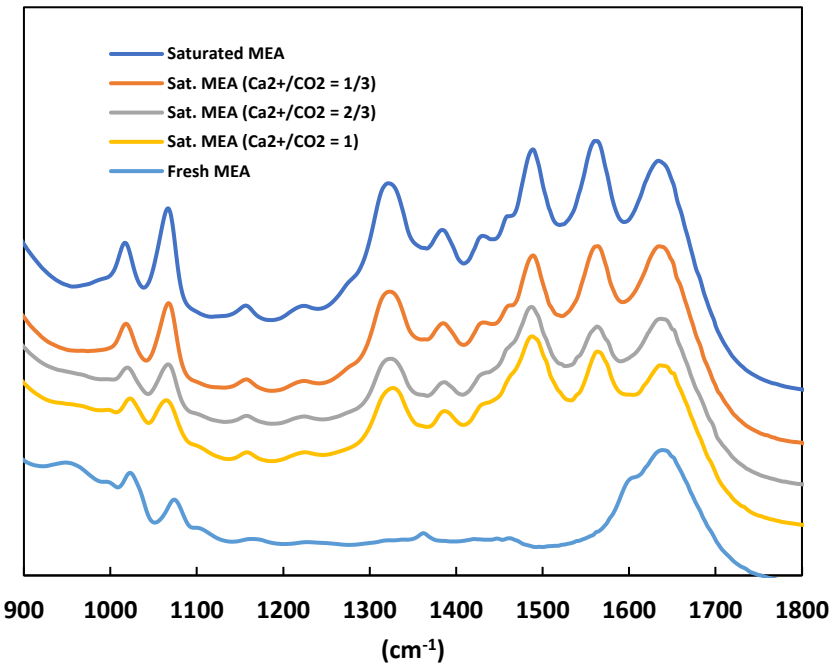

Figure 30: FT-IT analysis of MEA solutions treated with different amounts of CaO at 20 ^{o}C

5.2.4 Comparing the desorption/mineralization of different calcium precursors

In the previous section, the regeneration performances of different calcium precursors were assessed individually to study the effect of adding stoichiometric amounts of calcium to precipitate absorbed CO_2 in MEA solutions. To make a more consistent performance comparison between different calcium precursors, a fresh MEA solution of 200 ml was loaded with CO_2 using the same absorption criteria mentioned in previous sections then, the solution was divided into 50 ml portions. One portion was untreated saturated MEA and the rest three portions were each mixed with stoichiometric quantities of $Ca(OH)_2$, $CaCl_2$ and CaO, respectively. Then, all the four solutions were subject to the same regeneration conditions of heating at 80 ^{o}C for 40 minutes. The desorption isotherms for the four solutions and a summary of the results are shown in figure 31 and table 8. From the results it can be seen that the addition of $Ca(OH)_2$ and CaO seized the gaseous

desorption of CO_2 whereas adding $CaCl_2$ would still allow some amount to be desorbed in the gas. These results agreed with those obtained from the previous analysis considering each precursor individually.

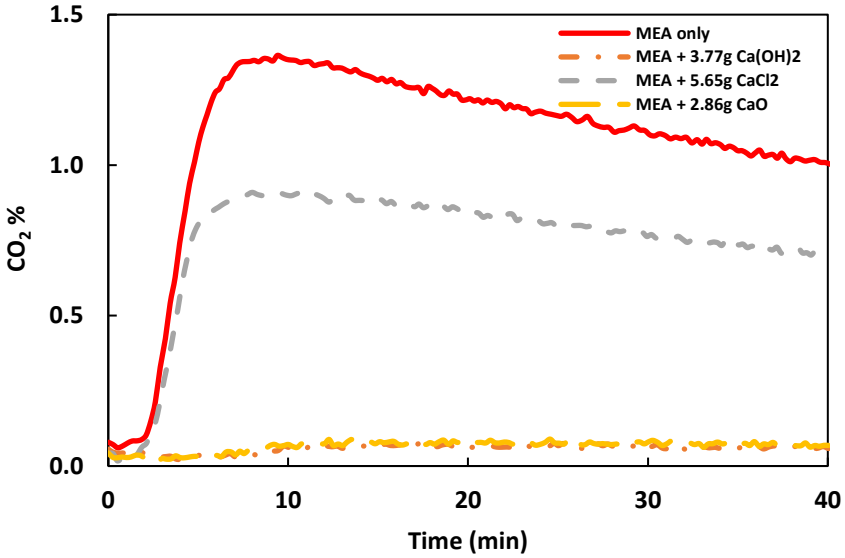

Figure 31: Desorption isotherms for MEA solutions regenerated with stoichiometric amounts of $Ca(OH)_2$, CaO and $CaCl_2$ at 80 ^oC for 40 min.

Table 8: Experimental results of regenerating MEA with stoichiometric amounts of $Ca(OH)_2$, CaO and $CaCl_2$ at 80 ^oC for 40 min.

Sample	Initial CO2 loading	Desorption *(Gas)*	Desorption *(Solid)*	CO_2 removed	Collected solids	Final CO2 loading
	[mol CO_2/mol MEA]			*[%]*	*[g]*	*[mol CO_2/mol MEA]*
MEA	**0.280**	0.054	0.000	19.4	-	**0.226**
MEA + 3.77 g $Ca(OH)_2$	**0.280**	0.003	0.244	88.0	4.454	**0.034**
MEA + 5.65 g $CaCl_2$	**0.280**	0.037	0.202	85.6	3.691	**0.040**
MEA + 2.86 g CaO	**0.280**	0.003	0.233	84.4	4.341	**0.044**

From the TGA results in figure 32, the weight loss of the solids (above 600 ^{o}C) resulting from the mineralization with $Ca(OH)_2$, $CaCl_2$ and CaO revealed that they were composed of 99.5, 99.6 and 98.2 wt% of $CaCO_3$, respectively. These results were further confirmed with the XRD results shown in figure 33 which shows that the solids generated from CaO and $CaCl_2$ resembled the diffraction patter of pure aragointe polymorph, whereas those generated from $Ca(OH)_2$ showed a calcite polymorph pattern. Just as expected from previous results with $Ca(OH)_2$ and CaO, table 8 shows that the majority of the absorbed CO_2 (86.9 mol% with $Ca(OH)_2$ and 83.6 mol% with CaO) were mineralized to $CaCO_3$ with almost no gas desorption. On the other hand, adding $CaCl_2$ mineralized 72.1 mol% of the absorbed CO_2 while 13.4 mol% were desorbed as a gas. Moreover, the total amount of CO_2 desorption far exceeded the desorption accomplished by thermal treatment alone which was less than 20 mol% of dissolved CO_2.

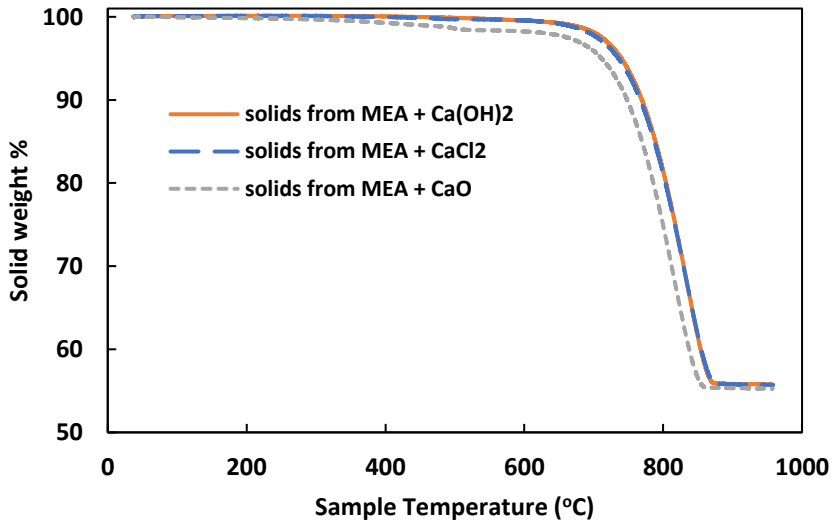

Figure 32: TGA results of the solids generated from adding stoichiometric amounts of different calcium precursors on saturated MEA at 80 ^{o}C

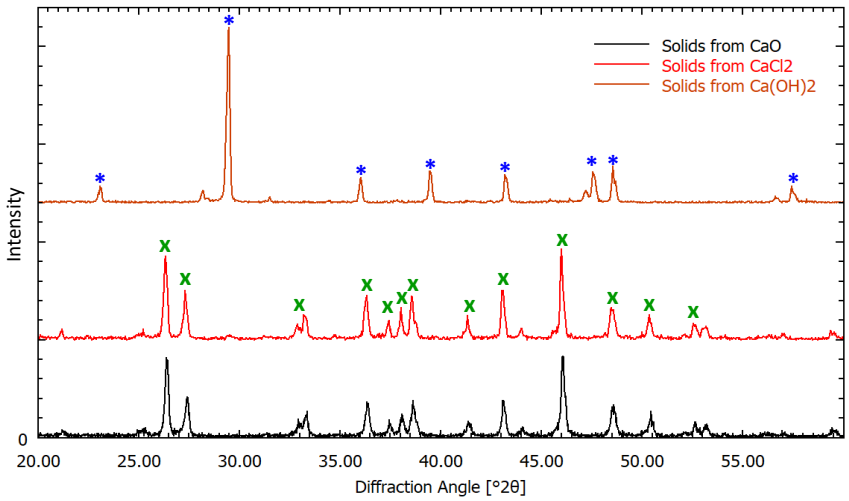

Figure 33:XRD diffraction patterns of the solids generated from regenerating MEA with stoichiometric amounts of $Ca(OH)_2$, $CaCl_2$ and CaO. The (*) signs correspond to characteristic peaks resembling calcite pattern. The (×) signs correspond to characteristic peaks resembling aragonite pattern.

The pH measurements (figure 34) for the initial and regenerated solutions shows that both $Ca(OH)_2$ and CaO resulted in a solution that had a similar high pH value of 11. However, regenerating with $CaCl_2$ resulted in a solution with a pH value of 9.7, which was lower than the pH value of the initial solution before the solid addition. Again, these results highlight the influence of Cl^- ions on the regeneration process.

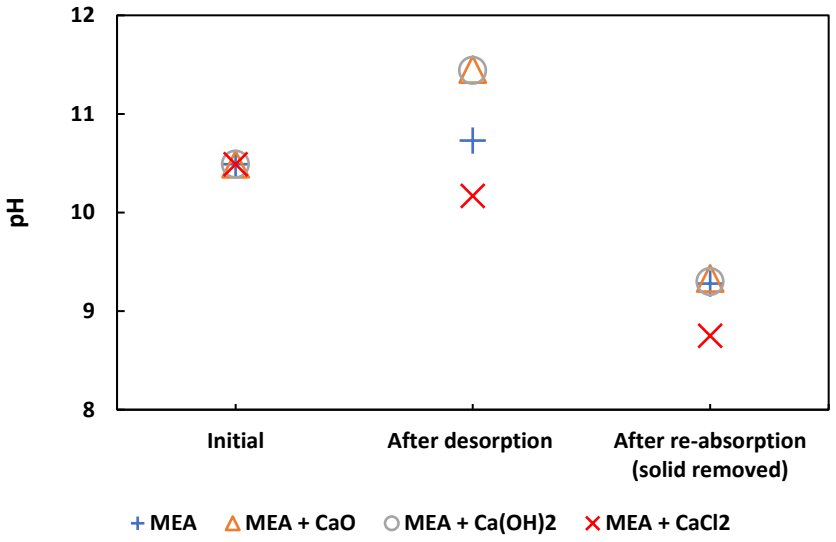

Figure 34: pH values of MEA solutions mixed with stoichiometric amounts of $Ca(OH)_2$, $CaCl_2$ and CaO and regenerated at 80 °C for 40 min.

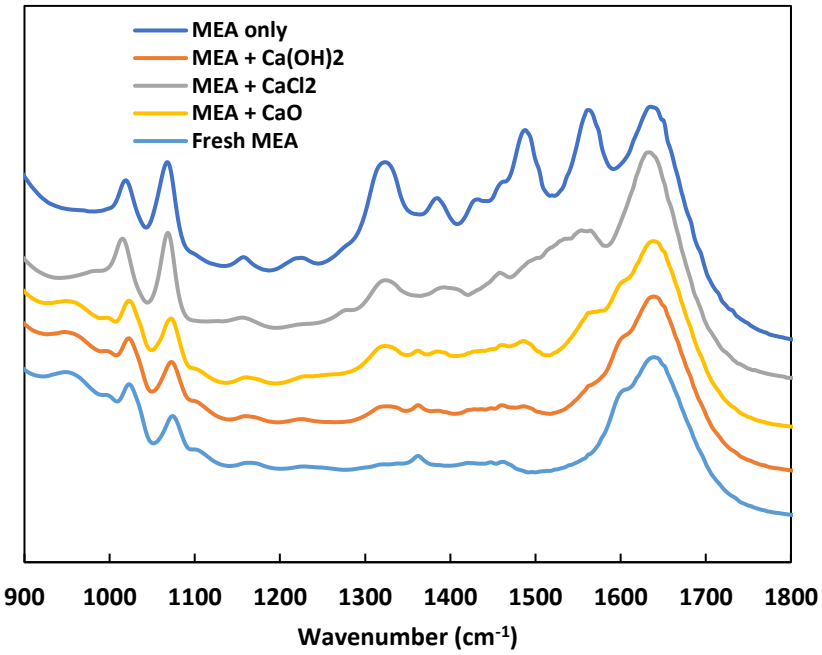

Figure 35: FT-IR spectra of MEA liquid samples regenerated with stoichiometric amounts of $Ca(OH)_2$, $CaCl_2$ and CaO at 80 °C for 40 minutes.

Figure 35 shows the FT-IR spectra of the four liquid solutions. As can be observed from the figure, there was a significant reduction in the intensities of the peaks associated with carbamate, bicarbonate, carbonate and protonated amine for the solutions treated with $Ca(OH)_2$ and CaO. On the other hand, the solution resulted from the regeneration with $CaCl_2$ shows large but slightly lower reduction in the peak intensities of carbamate, bicarbonate and carbonate with an increase in the intensities of the peaks associated with protonated MEA. These results clearly show the substantial improvement of the regeneration extent when mineralization was coupled with the thermal energy. Unlike the other two calcium precursors, $CaCl_2$ appeared to negatively impact the solution's chemistry due to the presence of Cl^- ions which tends to greatly alter the solution equilibrium by increasing the pH and possibly bonding with MEA. This impact was confirmed by the observed pH decrease below the value of all other solutions as seen in figure 34. On the contrary, the reabsorption of the solutions treated with $Ca(OH)_2$ and CaO brought their pH to a value that exactly matched the pH of the untreated MEA. This confirms the absence of free OH^- ions suggesting the chemical integrity of the solutions. Figure 36 shows the reabsorption isotherm for the three solutions after removing the solids and stopping the experiment when the CO_2 breakthrough concentration reached 12.5%. These results prove the high regeneration extent with $Ca(OH)_2$ and CaO as both of their solutions absorbed more than double the amount absorbed by untreated MEA. The only difference was that regenerating with $Ca(OH)_2$ would slightly dilute the MEA solution due to the addition of water in a molar amount equivalent to the calcium hydroxide added. Again, because the initial and final CO_2 loadings of the four MEA solutions were expected to lie on different saturation isotherm points, relative absorption comparison was not used. Instead, only absolute reabsorption amounts are shown on figure 36 for reference. In the case with $CaCl_2$ regeneration, the reabsorption capacity was lower than the untreated MEA. This result

further confirms the effect that Cl^- ions play in changing the solution equilibrium availing less free MEA ready for absorption.

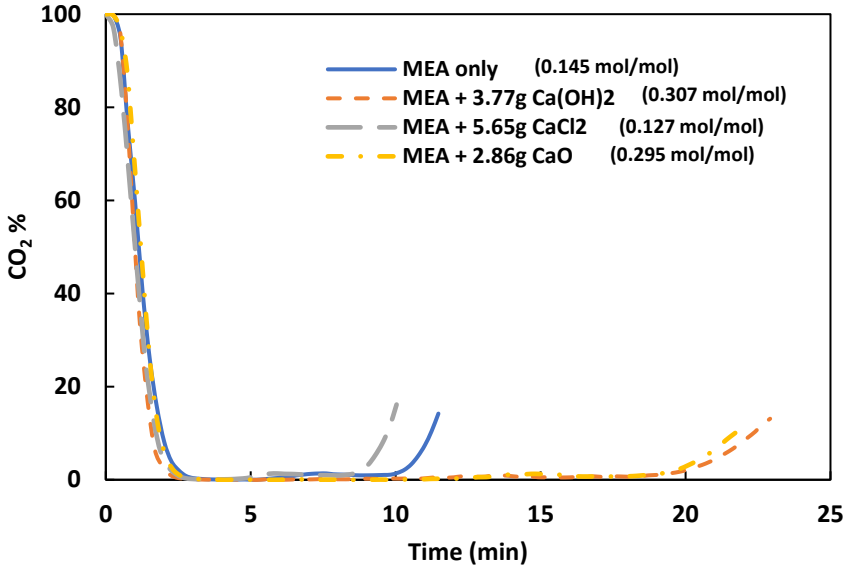

Figure 36: FT-IR spectra for the reabsorbed MEA solutions mixed with stoichiometric amounts of $Ca(OH)_2$, $CaCl_2$ and CaO after removing the solids.

5.2.5 Aspen Plus modeling of MEA absorption/desorption using $Ca(OH)_2$ and $CaCl_2$

Using the model described in section 4.7, a 22% MEA stream loaded with 0.5 mol CO_2/mol MEA (last column in table 3) was mixed with $Ca(OH)_2$ and $CaCl_2$ at Ca^{2+}/CO_2 ratios of 0.13 and 1.0 mol/mol while varying temperatures. This was done to note the effect of temperature on the mineralization process if different calcium precursors were used. As can be inferred from figure 37, 100% mineralization of calcium was observed irrespective of the reaction temperature. Contrary to our results which shows variation of mineralization extent with temperature (table 8 for example) especially for the case when $CaCl_2$ was used, this suggests that our experiments could have captured the transient condition where the mineralization rate could be greatly increased by

temperature. However, from the chemical equilibrium perspective, the model result indicates that CO_2 mineralization would always be preferred over gaseous desorption at our testing conditions.

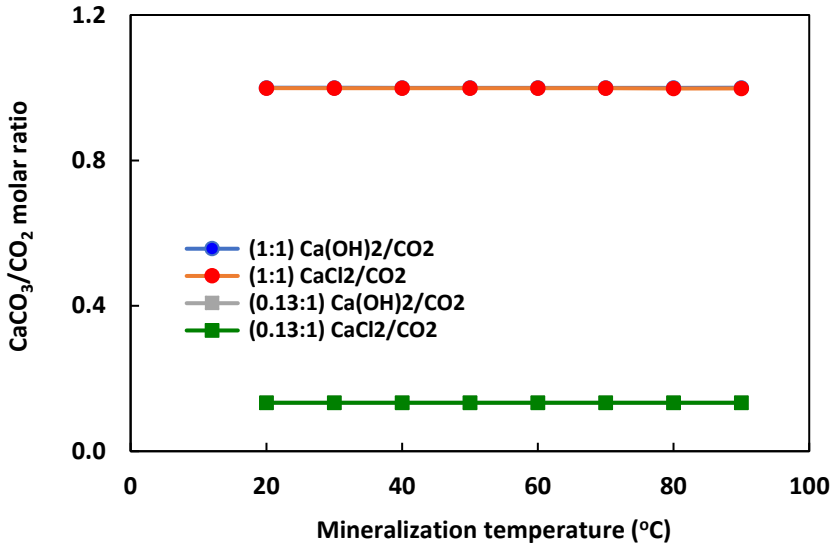

Figure 37: The effect of temperature change on the mineralization of CO_2 by mixing with $Ca(OH)_2$ and $CaCl_2$ at 0.13 and 1.0 mol Ca^{2+}/mol CO_2 ratios.

In this part, we looked at the flashing duty required to bring the loading of rich MEA from 0.5 mol/mol back to the loan loading of 0.33 mol/mol when different amounts of calcium were added. This was done by premixing the rich stream with $Ca(OH)_2$ and $CaCl_2$ in 0, 0.07, 0.13, and 0.27 Ca^{2+}/CO_2 ratios and noting the flashing duty required to desorb enough CO_2 in the gas and get the 0.33 mol/mol loading. As shown in figure 38, the CO_2 desorption energy decreases with the increase in the Ca^{2+}/CO_2 ratio for both precursors. This is because more CO_2 was removed by mineralization, as a more thermodynamically favored route, and the solution ended up with less CO_2 to desorb in the gas. The exothermic nature of the mineralization reaction was also observed to contribute to the overall reduction of the energy required for CO_2 desorption by making up part

of it. However, by comparing the duty trends in figure 38, it can be seen that adding $CaCl_2$ reduced the desorption duty much more than that from $Ca(OH)_2$. This could be explained by the solution's lower pH caused by the presence of free Cl- ions as opposed to the almost constant pH when $Ca(OH)_2$ was used (figure 39). Such lower alkalinity could be responsible for shifting the equilibrium of reaction (22) in the forward direction resulting in a gaseous release of CO_2 as observed from our experimental results.

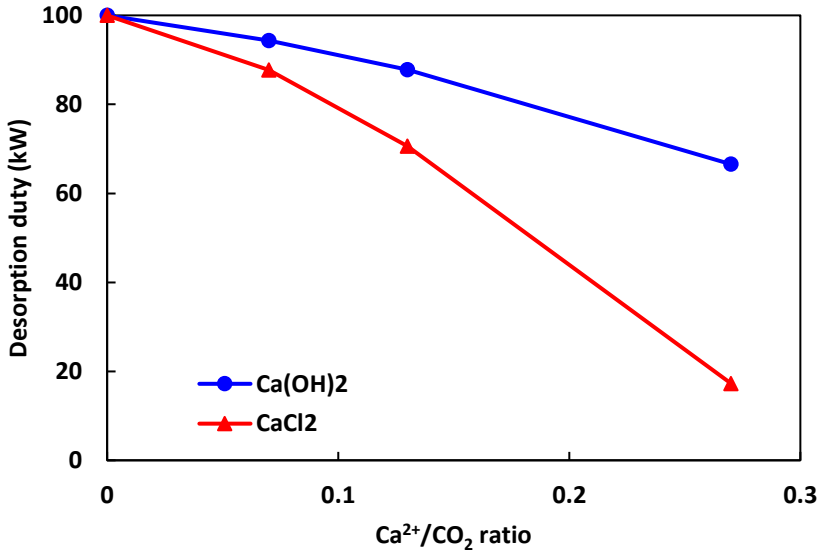

Figure 38: Duty to desorb CO_2 to the gas phase and bring the stream to the lean loading of 0.33 mol/mol when different molar ratios of $Ca(OH)_2$ and $CaCl_2$ were mixed.

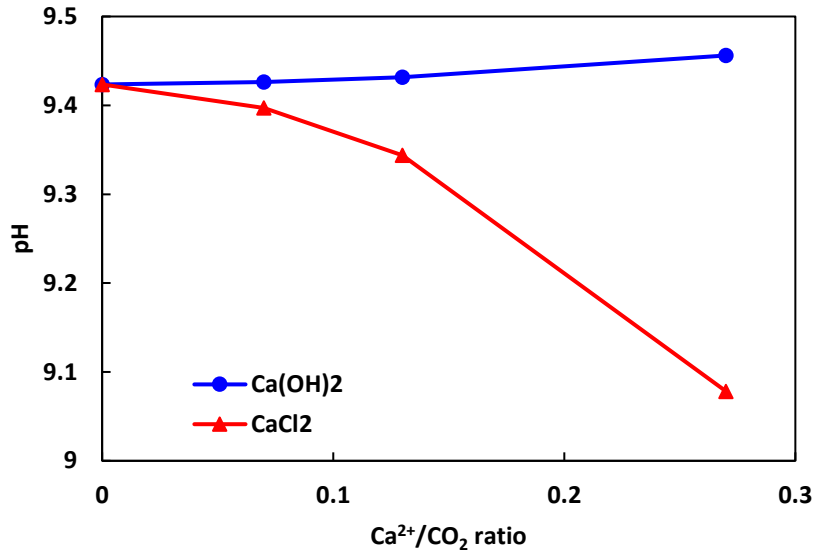

Figure 39: pH of the lean MEA stream (0.33 mol/mol loading) when different molar ratios of $Ca(OH)_2$ and $CaCl_2$ were used with the thermal regeneration.

To understand the impact of different calcium precursors on the reabsorption capacity, the compositions of the above lean solutions (with similar CO_2 loading of 0.33 mol/mol) were compared in figures 40 and 41. As can be inferred from the results, the composition of the solutions treated with $Ca(OH)_2$ didn't change after the absorption/desorption cycles. However, $CaCl_2$ was shown to alter the solutions equilibrium by producing more protonated MEA on the expense of unprotonated MEA. Again, this could be explained by the rising pH caused by the Cl^- ions in solution. This result also agrees with the FT-IR analysis done previously which revealed an increase in the peak associated with the protonated MEA when $CaCl_2$ was used for regeneration.

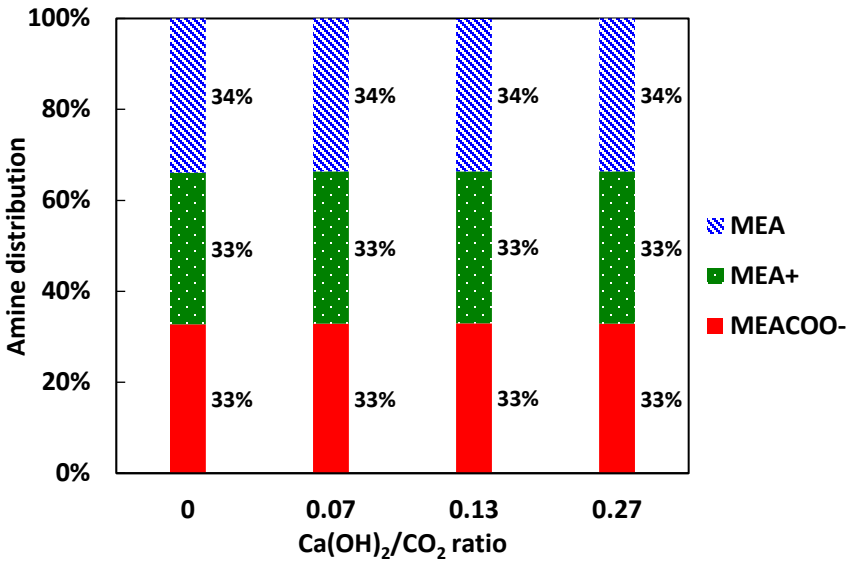

Figure 40: Composition of the lean MEA streams (0.33 mol/mol loading) when different molar ratios of $Ca(OH)_2/CO_2$ were used with the thermal regeneration.

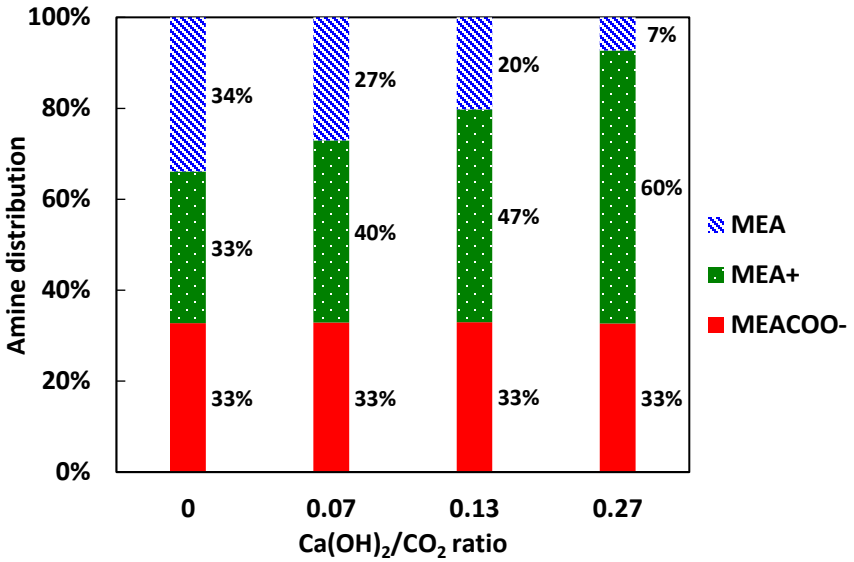

Figure 41: Composition of the lean MEA streams (0.33 mol/mol loading) when different molar ratios of $CaCl_2/CO_2$ were used with the thermal regeneration.

Figure 42 shows the percent of captured CO_2 from the flue gas when the above lean solutions underwent a second absorption cycles at 40 ^oC. As confirmed by the experimental results,

figure 42 shows that treating MEA streams with $Ca(OH)_2$ didn't have a notable impact on the reabsorption ability of MEA as 100% of the CO_2 in the flue gas was captured. On the other hand, the streams treated with $CaCl_2$ were seen to lose their ability to reabsorb CO_2 when as more salt was used to regenerate MEA in the preceding cycle. This was expected considering the lack of unprotonated MEA in the solutions containing Cl^- and from the experimental findings confirming the lower reabsorption ability.

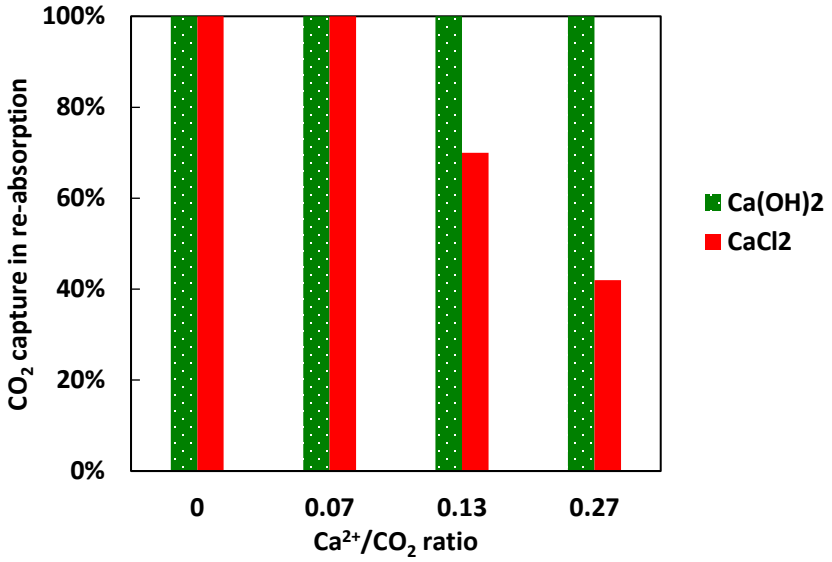

Figure 42:Percent CO_2 absorbed when the streams regenerated with different molar ratios of $Ca(OH)_2$ and $CaCl_2$ were re-absorbed with CO_2 in the flue gas

5.2.6 Testing for absorption/desorption mass transfer enhancement.

Because the objective of this study was to attempt to regenerate MEA with a CO_2 loading where dissolved CO_2 was most stable and the absorption reaction has highest activity, all absorption experiments were conducted in a way that limits effective absorption process. Namely, a gas feed dip tube with a wide opening was used to create large bubbles. The increased bubble

size results in a decrease in the effective interfacial surface area between the gas and liquid resulting in a poor mass transfer which results in a reduced absorption rate (T. Wang et al. 2016; W. Yu et al. 2019). Also, the absorption experiments were stopped when the outlet breakthrough concentration reached 12.5%. However, using these conditions, it was difficult to quantify any mass transfer enhancements associated with the presence of the solid particles during CO_2 absorption or desorption. This was particularly true considering that pervious experiments used high purity CO_2 gas and it is well known that high gas concentrations makes the gas absorption much easier compared to more diluted gases (Koytsoumpa, Bergins, and Kakaras 2018). Moreover, the large bubble size and the poor gas mixing were expected to significantly underestimate any improvements caused by solid particles addition. To test the influence of adding solid particles on the performance of the desorption of CO_2 from saturated MEA, a solution of 100 ml of fresh MEA was saturated with CO_2 following the same experimental protocol used in previous sections. Then, the saturated solution was divided into two 50 ml portions with one mixed with 1.0g of fine $CaCO_3$. These solutions were then subject to the same regeneration conditions of heating to 80 ^oC while stirring for 40 min. Figure 43 shows the desorption isotherm of the two solutions.

As can be seen from the results in table 9, the CO_2 desorption amounts were not greatly increased by the addition of the fine $CaCO_3$ particles. As such, adding 1.0 g (2 wt.%) of the solid increased the desorption by only 2.8 mol% relative to solid-free MEA. These results clearly show the limited ability of the setup to realize the added benefit of solid particles present in the solution.

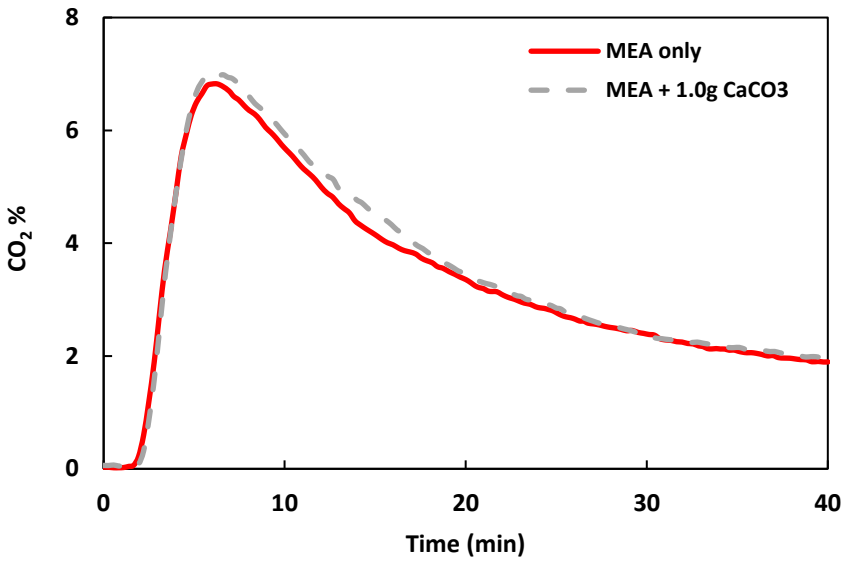

Figure 43: Desorption isotherms for CO_2-loaded MEA solutions mixed with 0 and 1.0 g of $CaCO_3$

Table 9: Experimental results for desorbing CO_2 from saturated MEA using 2 wt% of $CaCO_3$ solid particles

Sample	Feeding method	Initial solution loading	CO_2 removed *(Gas)*	CO_2 removed *(Solid)*	Increase in CO_2 removal	Gas desorption enhancement factor
		[mol CO_2/mol MEA]			*[%]*	*[-]*
MEA	Bubble tube	0.404	0.109	-		**1.00**
MEA + 1.0g $CaCO_3$	Bubble tube	0.404	0.112	-	2.8	**1.02**
MEA	Gas sparger	0.321	0.050	-	-	**1.00**
MEA + 1.0g $CaCO_3$	Gas sparger	0.321	0.058	-	15.1	**1.20**
MEA + 0.74g $Ca(OH)_2$	Gas sparger	0.321	0.032	0.054	70.1	**0.59**

In order to actively realize the benefit of adding the solid particles in MEA solutions, it was necessary to operate the rector at conditions that makes the reaction more diffusion limited. To accomplish this, higher flow rates of the feed gas were used in addition to reducing the CO_2 concentration in feed to 13 vol%. Moreover, a gas sparger was used in place of the dip tube to

provide a better gas dispersion. In this experiment, a sample of 150 ml of MEA was bubbled with CO_2 until reaching a breakthrough concentration of 7.5 vol% in the outlet gas. The saturated solution was then divided into three 50 ml portions two of which were mixed with 1.0g $CaCO_3$ and 0.74g $Ca(OH)_2$. The latter amount corresponded to the amount of $Ca(OH)_2$ making 1.0 g of $CaCO_3$ upon mineralization in solution. Then, all the three solutions were regenerated at 80-81 ^oC for 30 minutes. It is worth stating $CaCl_2$ was excluded from our analysis to rule out the effect of Cl^- on the regeneration experiment. The regeneration isotherm and the summary of the results are shown in figure 44 and table 9.

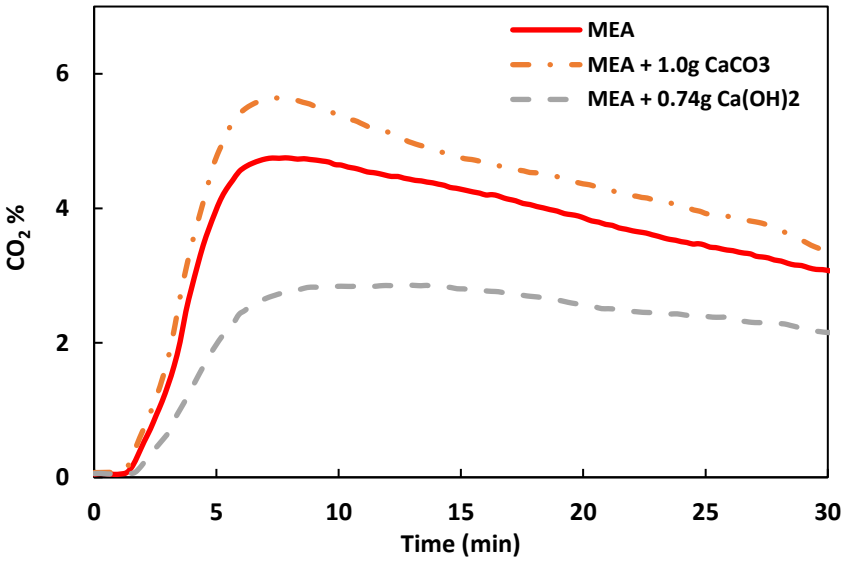

Figure 44: CO_2 desorption from MEA using gas feed dip tube and 2 wt% $CaCO_3$ solid particles

As can be seen from the results of table 9, changing the experimental setup resulted in magnifying the effect of the solid particles in the desorption process. In this case, adding 2 wt% of $CaCO_3$ particles in solution resulted in 15.1 mol% increase in the desorption amount compared to

the solid-free MEA. In addition, the gas desorption enhancement factor for the MEA solution mixed with 1.0g of $CaCO_3$ (calculated from equation 32) showed an order of magnitude improvement over the untreated solution. Moreover, adding $Ca(OH)_2$, which corresponded to making 2 wt% $CaCO_3$ in solution, increased the total CO_2 removal by 70.1 mol%. This was due to the combined effect of the chemical mineralization of absorbed CO_2 in addition to the gaseous desorption caused by solid particles enhancement. However, the solution treated with $Ca(OH)_2$ showed a much lower gas desorption enhancement factor than the solid-free MEA solution. This was expected knowing that this solution had a much lower CO_2 content due to mineralization.

To confirm the absorption and desorption enhancement caused by the presence of solid particles, another absorption and desorption cycle was conducted for all the three solutions without removing the solids. Figure 45 shows the absolute CO_2 absorption and removal amounts for all the three solutions. It is important to note that these experiments didn't consider the full saturation/desorption of MEA solutions and therefore, each treated solution had slightly different starting/ending saturation isotherm points. It can be observed from figure 45 that while using similar absorption and desorption conditions for all solutions, the samples with the 2 wt% solids gave higher absorption and desorption amounts of CO_2 above those given off by solid-free MEA. This was expected knowing that the solutions were partially regenerated and that the solid particles only change the kinetics of reaction and not the equilibrium. Figure 46 compares the enhancement factor for all the three solutions during both absorption and desorption cycles. The result shows that incorporating $CaCO_3$ solid particles also improved the enhancement factors for both the second absorption and desorption processes. Also, by comparing the enhancement factors of the two solid-loaded MEA solutions (figure 46) the solution with the $CaCO_3$ generated from mineralization had a notably higher enhancement factor in the second absorption (6 and 9%

increase) and desorption (15 and 20% increase) cycles. This improvement was potentially a result of the differences in the initial CO_2 loadings before each process step caused by the mineralization reaction. Another possible explanation was that the mineralization-generated $CaCO_3$ might had a different particle size than those in the other solution which made a more pronounced gas-liquid mass transfer improvement.

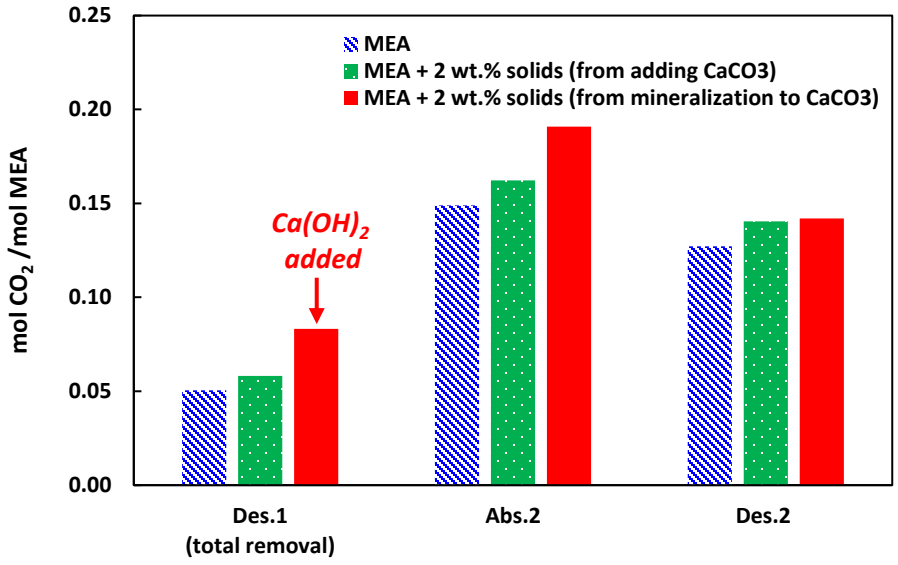

Figure 45: Comparison of the absolute CO_2 absorption and desorption amounts when saturated MEA was mixed with 2 wt% of $CaCO_3$ by directly adding $CaCO_3$ in solution (green bars) or by in-situ generation of $CaCO_3$ particles through mineralization (red bars).

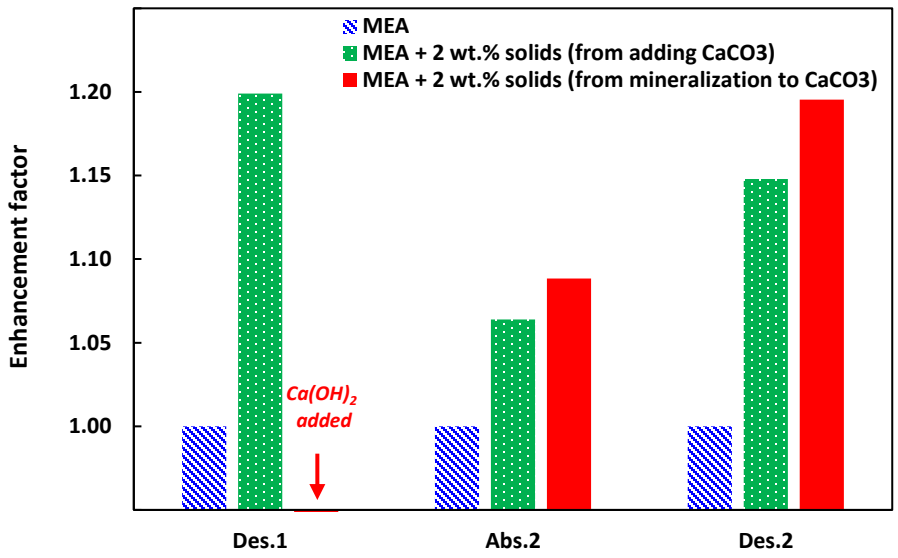

Figure 46: Comparison of the CO_2 gas absorption and desorption enhancement factors for each step

Because the majority of the CO_2 was desorbed during the first 15 minutes of the regeneration process, the relative mass transfer interfacial areas comparing the solid-loaded and unloaded MEA solution were calculated by averaging the interfacial areas within every 5 minutes (of the 15 minutes) and taking their ratio. Using equation 31, the average ratios of the interfacial surface areas were calculated for the second desorption cycle, where the solutions had comparably the same initial CO_2 loading, and are compared in figure 47. The results show that during the first 5 min of desorption, the solution containing the mineralized $CaCO_3$ had a significant interfacial area increase of 56% while the solution with the added $CaCO_3$ had a 29% increase over the solid-free solution. These results clearly reveal the contribution of the solid particles in enhancing the CO_2 desorption by allowing faster transport from the liquid phase. Because the presence of the solid particles was expected to influence the kinetics of the desorption process and not the

equilibrium, the effective surface interfacial area ratio was diminishing past the first 5 min as the desorption proceeded. Tables 10 - 12 shows the experimental data used to generate these plots.

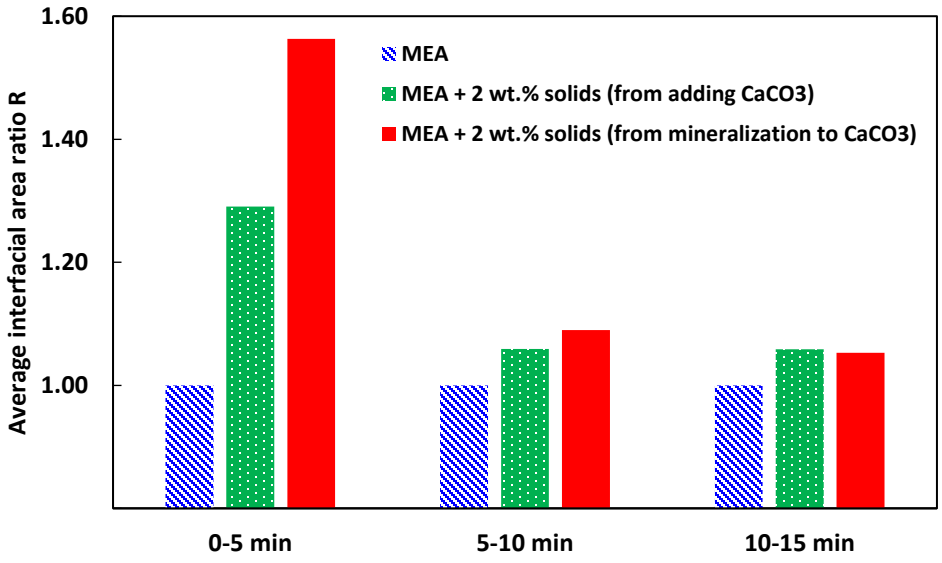

Figure 47: Comparison of the relative interfacial surface area between CO_2 and MEA within 5 min intervals during the first 15 min desorption time.

Table 10: Experimental data for the first 15 min of desorption for the solid-free MEA solution at 80°C.

Time [min]	x [%]	$N_{CO_2,G}$ [moles] $\times 10^4$	n_{CO_2} [mole/min] $\times 10^4$	P_{CO_2} [atm] $\times 10^3$	$A_{no\ solids}$ [m^2] $\times 10^8$
0.0	0.0	0.0	0.0	0.2	0.2
0.3	0.0	0.0	0.0	0.2	0.2
0.6	0.0	0.0	0.0	0.2	0.2
0.9	0.0	0.0	0.0	0.2	0.2
1.2	0.0	0.1	0.0	0.2	0.2
1.5	0.1	0.1	0.0	0.4	0.3
1.8	0.4	0.1	0.2	1.9	1.1
2.1	1.4	0.4	0.7	6.8	4.2
2.5	3.0	1.0	1.9	15.2	10.7

2.8	5.1	2.1	3.5	25.5	20.2
3.1	7.4	3.7	5.6	37.2	31.9
3.3	9.4	5.6	7.6	47.1	44.0
3.6	11.1	7.9	9.5	55.6	54.9
3.8	12.5	11.1	11.1	62.6	64.6
4.1	14.1	15.0	12.8	70.6	74.4
4.4	15.3	19.2	14.4	76.6	84.1
4.8	16.2	24.1	15.5	80.9	91.7
5.1	17.0	29.2	16.5	85.1	98.3
5.4	17.4	34.2	17.3	86.8	103.2
5.7	17.4	39.7	17.5	87.1	105.5
6.0	17.3	45.1	17.5	86.7	106.2
6.3	17.1	50.8	17.3	85.7	106.0
6.6	16.8	56.2	17.0	84.0	104.8
6.9	16.2	61.5	16.4	81.1	102.2
7.3	15.8	66.6	15.8	79.0	99.2
7.6	15.4	71.1	15.4	77.0	96.8
7.9	15.0	75.8	14.9	75.0	94.5
8.2	14.6	80.8	14.4	72.9	92.2
8.5	14.2	85.4	13.9	70.8	89.7
8.9	13.7	89.9	13.5	68.6	87.2
9.2	13.3	94.5	13.0	66.5	84.7
9.6	13.0	98.4	12.6	64.8	82.4
9.9	12.5	102.9	12.1	62.5	80.1
10.3	12.2	106.8	11.7	60.9	77.7
10.6	11.9	110.5	11.4	59.3	75.8
10.9	11.6	113.9	11.0	57.8	74.0
11.2	11.3	117.1	10.7	56.4	72.3
11.5	11.0	120.3	10.4	54.9	70.6
11.8	10.7	123.2	10.1	53.6	68.9
12.1	10.5	126.1	9.8	52.3	67.3
12.4	10.1	129.5	9.5	50.7	65.7
12.7	9.9	132.1	9.3	49.5	64.0
13.0	9.7	134.9	9.0	48.3	62.5
13.4	9.4	137.8	8.8	47.1	61.1
13.6	9.2	140.3	8.5	45.9	59.6
14.0	9.0	142.8	8.3	44.8	58.3
14.3	8.7	145.3	8.1	43.6	56.9
14.6	8.5	147.8	7.9	42.7	55.6
14.9	8.3	150.3	7.7	41.6	54.4

Table 11: Experimental data for the first 15 min of desorption for the MEA solution with 2wt.% $CaCO_3$ added solid particles at 80^{o}C.

Time [min]	x [%]	$N_{CO_2,G}$ [moles] $\times 10^4$	n_{CO_2} [mole/min] $\times 10^4$	P_{CO_2} [atm] $\times 10^3$	A_{solids} [m^2] $\times 10^8$
0.0	0.1	0.0	0.1	0.5	0.4
0.2	0.1	0.0	0.1	0.4	0.4
0.5	0.1	0.1	0.1	0.4	0.4
0.8	0.1	0.1	0.1	0.4	0.4
1.0	0.1	0.1	0.1	0.4	0.4
1.2	0.2	0.1	0.1	0.9	0.6
1.5	0.9	0.2	0.5	4.7	2.6
1.7	2.1	0.6	1.3	10.4	7.2
2.0	4.0	1.2	2.6	19.8	14.6
2.2	6.0	2.3	4.3	29.8	24.5
2.5	8.2	4.0	6.4	41.2	36.0
2.8	10.3	6.1	8.5	51.4	48.2
3.0	12.2	8.9	10.5	61.0	60.0
3.3	14.2	12.1	12.7	71.2	72.5
3.5	15.8	16.1	14.7	78.8	84.4
3.8	17.4	22.1	16.5	87.2	96.0
4.2	18.7	29.4	18.3	93.7	107.5
4.6	19.4	37.2	19.6	96.9	115.9
5.0	19.5	43.9	20.1	97.7	120.0
5.3	19.4	51.0	20.1	97.0	121.3
5.7	19.1	58.4	19.8	95.3	120.7
6.0	18.6	66.1	19.3	92.9	118.8
6.4	18.0	72.5	18.6	89.9	115.6
6.8	17.4	77.6	17.8	86.9	111.8
7.1	16.9	82.2	17.2	84.7	108.6
7.3	16.5	86.6	16.7	82.7	106.1
7.6	15.9	90.8	16.1	79.4	102.7
7.8	15.5	94.7	15.5	77.7	99.5
8.1	15.1	98.6	15.0	75.5	97.1
8.4	14.8	102.2	14.6	73.8	94.8
8.6	14.4	106.0	14.2	71.8	92.6
8.9	14.0	109.8	13.8	70.2	90.4
9.1	13.7	113.2	13.4	68.4	88.3
9.4	13.4	116.5	13.0	66.9	86.3
9.7	13.1	119.6	12.7	65.4	84.5
9.9	12.8	122.7	12.4	64.2	83.0

10.2	12.5	125.9	12.0	62.4	81.1
10.4	12.2	129.0	11.7	61.2	79.2
10.7	12.0	131.9	11.4	59.8	77.7
10.9	11.7	134.8	11.2	58.7	76.2
11.2	11.5	137.8	10.9	57.5	74.9
11.5	11.3	140.5	10.7	56.4	73.6
11.7	11.1	143.1	10.5	55.4	72.3
12.0	10.9	145.9	10.3	54.4	71.2
12.2	10.7	148.6	10.0	53.4	70.1
12.5	10.5	151.1	9.8	52.4	68.9
12.8	10.3	153.5	9.6	51.5	67.7
13.0	10.1	155.9	9.4	50.5	66.6
13.3	10.0	158.1	9.3	49.8	65.6
13.5	9.8	160.5	9.1	49.0	64.8
13.8	9.6	162.7	9.0	48.2	63.9
14.0	9.5	164.9	8.8	47.6	63.1
14.3	9.4	167.3	8.7	46.9	62.4
14.5	9.3	169.4	8.5	46.3	61.6
14.8	9.1	171.6	8.4	45.6	60.9
15.0	9.0	173.7	8.3	44.9	60.2

Table 12: Experimental data for the first 15 min of desorption for the MEA solution with 2wt.% $CaCO_3$ solid particles from in-solution CO_2 mineralization 80°C.

Time [min]	x [%]	$N_{CO_2,G}$ [moles] $\times 10^4$	n_{CO_2} [mole/min] $\times 10^4$	P_{CO_2} [atm] $\times 10^3$	A_{solids} [m^2] $\times 10^8$
0.0	0.1	0.0	0.1	0.3	0.3
0.3	0.1	0.0	0.1	0.4	0.3
0.5	0.1	0.0	0.1	0.3	0.3
0.8	0.1	0.1	0.1	0.3	0.3
1.1	0.1	0.1	0.1	0.3	0.3
1.3	0.2	0.1	0.1	1.0	0.6
1.5	0.9	0.2	0.5	4.6	2.6
1.8	2.3	0.6	1.4	11.6	7.6
2.1	4.4	1.3	2.9	21.8	16.0
2.3	6.7	2.6	4.8	33.3	27.2
2.6	8.9	4.2	7.0	44.7	39.5
2.8	11.0	6.3	9.2	54.9	51.8
3.0	13.0	9.1	11.3	65.2	64.2
3.3	14.8	12.4	13.4	74.0	76.3
3.5	16.3	15.9	15.3	81.5	87.3
3.8	17.7	20.4	17.0	88.7	97.9

4.0	18.7	24.9	18.5	93.7	107.1
4.3	19.5	29.8	19.6	97.3	114.1
4.5	19.9	35.1	20.4	99.6	119.4
4.8	20.1	40.2	20.8	100.5	122.6
5.0	20.1	45.5	20.9	100.7	124.3
5.3	20.0	50.7	20.9	99.9	124.7
5.5	19.7	55.9	20.6	98.7	124.1
5.8	19.4	61.4	20.2	97.1	122.9
6.0	18.9	66.2	19.7	94.7	120.5
6.3	18.6	71.2	19.2	93.0	118.1
6.5	18.2	75.8	18.8	91.1	116.1
6.8	17.8	80.4	18.3	89.0	113.8
7.1	17.3	85.0	17.7	86.6	111.1
7.3	16.9	89.4	17.2	84.7	108.5
7.6	16.5	93.4	16.7	82.6	106.1
7.8	15.9	97.6	16.1	79.4	102.7
8.1	15.5	101.5	15.5	77.6	99.5
8.3	15.1	105.3	15.0	75.7	97.2
8.6	14.7	108.7	14.6	73.6	94.8
8.8	14.4	112.0	14.2	72.0	92.5
9.0	14.1	115.4	13.8	70.4	90.5
9.3	13.8	118.6	13.5	69.0	88.8
9.5	13.5	122.0	13.2	67.6	87.2
9.8	13.2	125.3	12.8	65.9	85.4
10.0	12.9	128.4	12.5	64.5	83.5
10.3	12.5	131.6	12.1	62.6	81.4
10.5	12.2	134.5	11.7	61.2	79.3
10.8	12.0	137.6	11.4	59.8	77.7
11.1	11.7	140.3	11.2	58.6	76.1
11.3	11.5	143.1	10.9	57.5	74.7
11.6	11.3	145.9	10.7	56.3	73.4
11.8	11.1	148.4	10.4	55.3	72.0
12.1	10.9	151.0	10.2	54.3	70.9
12.3	10.6	153.4	10.0	53.2	69.7
12.6	10.5	156.0	9.8	52.3	68.5
12.8	10.2	158.4	9.6	51.2	67.3
13.1	10.0	160.7	9.4	50.0	65.9
13.3	9.8	163.0	9.2	49.1	64.7
13.6	9.6	165.2	9.0	48.2	63.6
13.8	9.4	167.5	8.8	47.2	62.4
14.1	9.3	169.6	8.6	46.3	61.2
14.3	9.1	171.7	8.4	45.4	60.2
14.6	8.9	173.8	8.2	44.5	59.0
14.8	8.7	175.7	8.0	43.7	58.0

6 Conclusion

Even though MEA solutions have superior CO_2 capturing properties, they still suffer from the high thermal energy required for regeneration. Mineralizing absorbed CO_2 by mixing the saturated MEA solutions with different calcium precursors is an appealing method considering the fast mineralization reaction and the ability to capture CO_2 in a thermodynamically stable form of $CaCO_3$. However, the high stability of carbamate species in saturated MEA solutions would limit the mineralization reaction resulting in a low regeneration extent. Attempting to mineralize the absorbed CO_2 while heating the saturated MEA solution to 80 ^oC was found to significantly improve the mineralization reaction and increase the $CaCO_3$ yield while significantly reducing the CO_2 content in solution. More specifically, adding stoichiometric amounts of $Ca(OH)_2$, CaO and $CaCl_2$, (to balance the absorbed CO_2 in MEA) while heating the rich MEA solutions brought their CO_2 loading to below 0.045 mol/mol ratio. $Ca(OH)_2$ and CaO mineralized 86.9 mol% and 83.6 mol% of the absorbed CO_2, respectively, with almost no gas desorption. On the other hand, $CaCl_2$ was found to mineralize 72.1 mol% of the absorbed CO_2 while 13.4 mol% were desorbed as a gas. The presence of chlorine ions was found to reduce the alkalinity of the MEA solution which might resulted in a reaction equilibrium shift that increased the gaseous CO_2 desorption during regeneration. The second absorption cycles and the pH results proved that the solutions mixed with $Ca(OH)_2$ and CaO had retained their high absorption capacities which was then confirmed by the Aspen Plus model. The only exception was that adding $Ca(OH)_2$ was expected to dilute the MEA solution as it brings a water molecule for every hydroxide molecule added. On the other hand, the presence of chlorine ions in the MEA solutions mixed with $CaCl_2$ had a detrimental effect on the reabsorption capacity of MEA especially when present in large quantities. The modeling results revealed that mixing rich MEA streams with calcium precursors could greatly reduce the energy

required for CO_2 desorption by: mineralizing CO_2 as more favorable route of removal, supplying additional regeneration heat though the exothermic mineralization reaction, and inducing a pH change making the CO_2 gaseous desorption less energetic (as in the case with $CaCl_2$).

Adding small amounts of calcium precursors (such as $Ca(OH)_2$) and heating at 82 ^oC was found to drastically improve the CO_2 removal process. This was explained by the combined effect of CO_2 mineralization while kinetically improving the desorption process with the generated solid particles. In addition, having these solid particles in solution was found to also improve the subsequent absorption and desorption cycles. More specifically, mineralization-generated solid particles were found to improve the absorption and desorption enhancement factors and interfacial liquid-gas contact area beyond those from normal $CaCO_3$ solid addition. Further investigation on the particle sizes of generated solids could explain their distinctive enhancement advantage. Overall, the study results proved the importance the thermal energy in driving the mineralization reaction. Additionally, mineralizing some of the absorbed CO_2 while maintaining some of the generated solids in solution could make a promising industrial advancement in reducing amine regeneration energy and increasing the overall CO_2 capture.

7 References

Adeosun, Adewale, Nabil El Hadri, Earl Goetheer, and Mohammad R M Abu-Zahra. 2013. "Absorption of CO2 by Amine Blends Solution: An Experimental Evaluation." *International Journal of Engineering and Science* 3 (9): 12–23.

Akachuku, Ananda, Priscilla Anima Osei, Benjamin Decardi-Nelson, Wayuta Srisang, Fatima Pouryousefi, Hussameldin Ibrahim, and Raphael Idem. 2019. "Experimental and Kinetic Study of the Catalytic Desorption of CO 2 from CO 2 -Loaded Monoethanolamine (MEA) and Blended Monoethanolamine – Methyl-Diethanolamine (MEA-MDEA) Solutions." *Energy* 179: 475–89. https://doi.org/10.1016/j.energy.2019.04.174.

Arti, Murnandari, Min Hye Youn, Ki Tae Park, Hak Joo Kim, Young Eun Kim, and Soon Kwan Jeong. 2017. "Single Process for CO2 Capture and Mineralization in Various Alkanolamines Using Calcium Chloride." *Energy and Fuels* 31 (1): 763–69. https://doi.org/10.1021/acs.energyfuels.6b02448.

Caplow, Michael. 1968. "Kinetics of Carbamate Formation and Breakdown." *Journal of the American Chemical Society* 90 (24): 6795–6803. https://doi.org/10.1021/ja01026a041.

Chang, Ribooga, Semin Kim, Seungin Lee, Soyoung Choi, Minhee Kim, and Youngjune Park. 2017. "Calcium Carbonate Precipitation for CO2 Storage and Utilization: A Review of the Carbonate Crystallization and Polymorphism." *Frontiers in Energy Research* 5 (July): 1–12. https://doi.org/10.3389/fenrg.2017.00017.

Declet, A., E. Reyes, and O. M. Suárez. 2016. "Calcium Carbonate Precipitation: A Review of the Carbonate Crystallization Process and Applications in Bioinspired Composites." *Reviews on Advanced Materials Science* 44 (1): 87–107.

Du, Min. 2017. "Effect of PH on Desorption of CO2 from Alkanolamine - Rich Solvents." *AIP Conference Proceedings* 1864 (August). https://doi.org/10.1063/1.4992908.

Du, Min, Bo Feng, Hui An, Wenqiang Liu, and Li Zhang. 2012. “Effect of Addition of Weak Acids on CO2 Desorption from Rich Amine Solvents.” *Korean Journal of Chemical Engineering* 29 (3): 362–68. https://doi.org/10.1007/s11814-011-0184-4.

Dutcher, Bryce, Maohong Fan, and Armistead G. Russell. 2015. “Amine-Based CO 2 Capture Technology Development from the Beginning of 2013-A Review.” *ACS Applied Materials and Interfaces* 7 (4): 2137–48. https://doi.org/10.1021/am507465f.

Feng, Bo, Min Du, Timothy James Dennis, Kim Anthony, and Marc Jarrod Perumal. 2010. “Reduction of Energy Requirement of CO2 Desorption by Adding Acid into CO2-Loaded Solvent.” *Energy and Fuels* 24 (1): 213–19. https://doi.org/10.1021/ef900564x.

Galan, Isabel, Fredrik P. Glasser, and Carmen Andrade. 2013. “Calcium Carbonate Decomposition.” *Journal of Thermal Analysis and Calorimetry* 111 (2): 1197–1202. https://doi.org/10.1007/s10973-012-2290-x.

“Global Carbon Project (GCP).” n.d.

Hamidi, R., M. Farsi, and R. Eslamloueyan. 2018. “CO2 Solubility in Aqueous Mixture of MEA, MDEA and DAMP: Absorption Capacity, Rate and Regeneration.” *Journal of Molecular Liquids* 265: 711–16. https://doi.org/10.1016/j.molliq.2018.07.013.

Huertas, José I., Martin D. Gomez, Nicolas Giraldo, and Jessica Garzón. 2015. “CO $_2$ Absorbing Capacity of MEA.” *Journal of Chemistry* 2015 (2): 1–7. https://doi.org/10.1155/2015/965015.

Jakobsen, Jana Poplsteinova, Jostein Krane, and Hallvard F. Svendsen. 2005. “Liquid-Phase Composition Determination in CO2-H 2O-Alkanolamine Systems: An NMR Study.” *Industrial and Engineering Chemistry Research* 44 (26): 9894–9903. https://doi.org/10.1021/ie048813+.

Ji, Long, Hai Yu, Kangkang Li, Bing Yu, Mihaela Grigore, Qi Yang, Xiaolong Wang, Zuliang

Chen, Ming Zeng, and Shuaifei Zhao. 2018. “Integrated Absorption-Mineralisation for Low-Energy CO 2 Capture and Sequestration.” *Applied Energy* 225 (April): 356–66. https://doi.org/10.1016/j.apenergy.2018.04.108.

Jiang, Jiazong, Bo Zhao, Yuqun Zhuo, and Shujuan Wang. 2014. “Experimental Study of CO2 Absorption in Aqueous MEA and MDEA Solutions Enhanced by Nanoparticles.” *International Journal of Greenhouse Gas Control* 29: 135–41. https://doi.org/10.1016/j.ijggc.2014.08.004.

Kang, Ji Min, Arti Murnandari, Min Hye Youn, Wonhee Lee, Ki Tae Park, Young Eun Kim, Hak Joo Kim, Seong Pil Kang, Jung Hyun Lee, and Soon Kwan Jeong. 2018. “Energy-Efficient Chemical Regeneration of AMP Using Calcium Hydroxide for Operating Carbon Dioxide Capture Process.” *Chemical Engineering Journal* 335 (August 2017): 338–44. https://doi.org/10.1016/j.cej.2017.10.136.

Kanniche, Mohamed, René Gros-Bonnivard, Philippe Jaud, Jose Valle-Marcos, Jean Marc Amann, and Chakib Bouallou. 2010. “Pre-Combustion, Post-Combustion and Oxy-Combustion in Thermal Power Plant for CO2 Capture.” *Applied Thermal Engineering* 30 (1): 53–62. https://doi.org/10.1016/j.applthermaleng.2009.05.005.

Kim, Young Eun, Jin Ah Lim, Soon Kwan Jeong, Yeo Il Yoon, Shin Tae Bae, and Sung Chan Nam. 2013. “Comparison of Carbon Dioxide Absorption in Aqueous MEA, DEA, TEA, and AMP Solutions.” *Bulletin of the Korean Chemical Society* 34 (3): 783–87. https://doi.org/10.5012/bkcs.2013.34.3.783.

Koytsoumpa, Efthymia Ioanna, Christian Bergins, and Emmanouil Kakaras. 2018. “The CO2 Economy: Review of CO2 Capture and Reuse Technologies.” *Journal of Supercritical Fluids* 132 (January 2017): 3–16. https://doi.org/10.1016/j.supflu.2017.07.029.

Leung, Dennis Y.C., Giorgio Caramanna, and M. Mercedes Maroto-Valer. 2014. “An Overview of Current Status of Carbon Dioxide Capture and Storage Technologies.” *Renewable and*

Sustainable Energy Reviews 39: 426–43. https://doi.org/10.1016/j.rser.2014.07.093.

Lv, Bihong, Bingsong Guo, Zuoming Zhou, and Guohua Jing. 2015. "Mechanisms of CO2 Capture into Monoethanolamine Solution with Different CO2 Loading during the Absorption/Desorption Processes." *Environmental Science and Technology* 49 (17): 10728–35. https://doi.org/10.1021/acs.est.5b02356.

McCant, Darrell D. 2015. "Monoethanolamine."

Mondal, Monoj K. 2009. "Solubility of Carbon Dioxide in an Aqueous Blend of Diethanolamine and Piperazine." *Journal of Chemical and Engineering Data* 54 (9): 2381–85. https://doi.org/10.1021/je800774c.

Osei, Priscilla A., Ananda Akachuku, Benjamin Decardi-Nelson, Wayuta Srisang, Fatemeh Pouryousefi, Paitoon Tontiwachwuthikul, and Raphael Idem. 2017. "Mass Transfer Studies on Catalyst-Aided CO2 Desorption from CO2-Loaded Amine Solution in a Post-Combustion CO2 Capture Plant." *Chemical Engineering Science* 170: 508–17. https://doi.org/10.1016/j.ces.2017.02.004.

Pacheco, Manuel A., Shoichi Kaganoi, and Gary T. Rochelle. 2000. "CO2 Absorption into Aqueous Mixtures of Diglycolamine(R) and Methyldiethanolamine." *Chemical Engineering Science* 55 (21): 5125–40. https://doi.org/10.1016/S0009-2509(00)00104-4.

Putta, Koteswara Rao, Diego D.D. Pinto, Hallvard F. Svendsen, and Hanna K. Knuutila. 2016. "CO2 Absorption into Loaded Aqueous MEA Solutions: Kinetics Assessment Using Penetration Theory." *International Journal of Greenhouse Gas Control* 53: 338–53. https://doi.org/10.1016/j.ijggc.2016.08.009.

Rinprasertmeechai, Supitcha, Sumaeth Chavadej, Pramoch Rangsunvigit, and Santi Kulprathipanja. 2012. "Carbon Dioxide Removal from Flue Gas Using Amine-Based Hybrid Solvent Absorption." *International Journal of Chemical and Biological Engineering* 64 (4): 296–300.

Rochelle, Gary T. 2009. “Amine Scrubbing for CO2 Capture.” *Science* 325 (5948): 1652–54. https://doi.org/10.1126/science.1176731.

Shi, Huancong, Abdulaziz Naami, Raphael Idem, and Paitoon Tontiwachwuthikul. 2014. “Catalytic and Non Catalytic Solvent Regeneration during Absorption-Based CO2 Capture with Single and Blended Reactive Amine Solvents.” *International Journal of Greenhouse Gas Control* 26: 39–50. https://doi.org/10.1016/j.ijggc.2014.04.007.

Tong, Danlu, J. P.Martin Trusler, Geoffrey C. Maitland, Jon Gibbins, and Paul S. Fennell. 2012. “Solubility of Carbon Dioxide in Aqueous Solution of Monoethanolamine or 2-Amino-2-Methyl-1-Propanol: Experimental Measurements and Modelling.” *International Journal of Greenhouse Gas Control* 6: 37–47. https://doi.org/10.1016/j.ijggc.2011.11.005.

US EPA, OAR. n.d. “Overview of Greenhouse Gases.”

Velts, O., M. Uibu, J. Kallas, and R. Kuusik. 2011. “CO2 Mineral Trapping: Modeling of Calcium Carbonate Precipitation in a Semi-Batch Reactor.” *Energy Procedia* 4: 771–78. https://doi.org/10.1016/j.egypro.2011.01.118.

Wang, Tao, Wei Yu, Fei Liu, Mengxiang Fang, Muhammad Farooq, and Zhongyang Luo. 2016. “Enhanced CO 2 Absorption and Desorption by Monoethanolamine (MEA)-Based Nanoparticle Suspensions.” *Industrial and Engineering Chemistry Research* 55 (28): 7830–38. https://doi.org/10.1021/acs.iecr.6b00358.

Wang, Wenlong, Xin Liu, Peng Wang, Yanli Zheng, and Man Wang. 2013. “Enhancement of CO 2 Mineralization in Ca 2 + - / Mg 2 + -Rich Aqueous Solutions Using Insoluble Amine.” https://doi.org/10.1021/ie400284v.

Wu, Xiaomei, Yunsong Yu, Zhen Qin, and Zaoxiao Zhang. 2014. “The Advances of Post-Combustion CO2 Capture with Chemical Solvents: Review and Guidelines.” *Energy Procedia* 63: 1339–46. https://doi.org/10.1016/j.egypro.2014.11.143.

Ying, Jiru, and Dag A. Eimer. 2013. “Determination and Measurements of Mass Transfer Kinetics of CO2 in Concentrated Aqueous Monoethanolamine Solutions by a Stirred Cell.” *Industrial and Engineering Chemistry Research* 52 (7): 2548–59. https://doi.org/10.1021/ie303450u.

Yu, Bing, Hai Yu, Kangkang Li, Long Ji, Qi Yang, Xiaolong Wang, Zuliang Chen, and Mallavarapu Megharaj. 2018. “A Diamine-Based Integrated Absorption − Mineralization Process for Carbon Capture and Sequestration : Energy Savings , Fast Kinetics , and High Stability.” Research-article. *Environmental Science & Technology* 52: 13629–37. https://doi.org/10.1021/acs.est.8b04253.

Yu, Wei, Tao Wang, Ah Hyung Alissa Park, and Mengxiang Fang. 2019. “Review of Liquid Nano-Absorbents for Enhanced CO2 Capture.” *Nanoscale* 11 (37): 17137–56. https://doi.org/10.1039/c9nr05089b.

Zhang, Xiaowen, Rui Zhang, Helei Liu, Hongxia Gao, and Zhiwu Liang. 2018. “Evaluating CO 2 Desorption Performance in CO 2 -Loaded Aqueous Tri-Solvent Blend Amines with and without Solid Acid Catalysts.” *Applied Energy* 218 (January): 417–29. https://doi.org/10.1016/j.apenergy.2018.02.087.

Zhang, Xiaowen, Xin Zhang, Helei Liu, Wensheng Li, Min Xiao, Hongxia Gao, and Zhiwu Liang. 2017. “Reduction of Energy Requirement of CO2 Desorption from a Rich CO2-Loaded MEA Solution by Using Solid Acid Catalysts.” *Applied Energy* 202: 673–84. https://doi.org/10.1016/j.apenergy.2017.05.135.

Zhong, Xiang Zhang, Guo Cai Wang, Ying Wang, Xiao Qi Zhang, and Wen Cai Ye. 2010. “Monomeric Indole Alkaloids from the Aerial Parts of Catharanthus Roseus.” *Yaoxue Xuebao* 45 (4): 471–74.